AN ABSTRACT OF THE THESIS OF

Eric M. Walters for the degree of Honors Baccalaureate of Science in Mechanical Engineering presented on May 23, 2014. Title: Development of a Framework for Analyzing the Effects of a Micro Pin Fin Array on the Catalytic Combustion of Hydrogen in Micro-channels.

Abstract approved:

_____

Vinod Narayanan

An experimental framework for investigation of the effects of Micro Pin Fin Arrays (MPFA) on the fuel oxidation efficiency of catalytic combustion is presented in this thesis. Complete combustion of the fuel is essential for operation at maximum efficiency and high standards of environmental cleanliness desired in existing microscale combustion applications. Higher residence times can increase the conversion rate of fuel as there is more time for the reaction to occur. Flow around a staggered array of pin fins causes increased residence times over a plain rectangular microgap due to the impingement of the flow on pins and the slower wake region behind the pins. The framework consists of detailed infrared thermography of the MPFA to characterize the surface temperature, scanning electron microscopy to characterize the catalyst morphology, and Energy Dispersive X-ray Spectroscopy (EDAX) to characterize the elemental composition of the catalyst surface. In addition to the local measurements, gas chromatography was used to identify the composition of the exhaust gas. To test the framework, a preliminary experiment of two different pin fin array geometries were investigated at various combustion temperatures and residence times. Based on the results of the experiment, further refinement of the framework is proposed.

Keywords: Combustion, catalysis, hydrogen, pin fins, micro-channels

Contact Email Address: ericwalters051@gmail.com

Development of a Framework for Analyzing the Effects of a Micro Pin Fin Array on the Catalytic Combustion of Hydrogen in Micro-channels

by

Eric M. Walters

A PROJECT

submitted to

Oregon State University

University Honors College

in partial fulfillment of
the requirements for the
degree of

Honors Baccalaureate of Science in Mechanical Engineering (Honors Scholar)

Presented May 23, 2014
Commencement June 2014

Honors Baccalaureate of Science in Mechanical Engineering thesis of Eric M. Walters presented on May 23, 2014.

APPROVED:

_____

Mentor, representing Mechanical Engineering

_____

Committee Member, representing Mechanical Engineering

_____

Committee Member, representing Mechanical Engineering

_____

Dean, University Honors College

I understand that my project will become part of the permanent collection of Oregon State University, University Honors College. My signature below authorizes release of my project to any reader upon request.

_____

Eric M. Walters, Author

Acknowledgement

I would like to extend my most sincere gratitude to anyone who has been even marginally involved with or has helped me to complete this research project.

I want to thank Dr. Vinod Narayanan, my thesis mentor, who guided me through the research and thesis writing process.

I would like to offer a very special thanks to Dr. Mohammad Ghazvini, who with supreme patience and generosity, mentored me from start to finish of my thesis project. Without him I would have been completely overwhelmed and I owe him my profound gratitude for donating his time and energy to my thesis project.

Finally, I would like to thank Emma McGuiness, who offered her never-ending love and support through long nights of data collection, analysis, and writing. I consider myself fortunate to have had her by my side through this arduous journey.

Table of Contents

Table of Contents (Cont.)

List of Figures

List of Figures (Cont.)

List of Tables

Development of a Framework for Analyzing the Effects of a Micro Pin Fin Array on the Catalytic Combustion of Hydrogen in Micro-channels

1 Introduction and Objectives

Chemical reactions are used in nearly every industry imaginable, from the creation of pharmaceuticals to the refining of raw petroleum to the generation of heat energy through combustion. It is of great interest to increase the rate at which reactions are completed while decreasing the size of the plant required to perform them. Recent advances in precision manufacturing have allowed researchers to develop very compact chemical reactors using arrays of micro-scale channels coated with a catalyst material. The small channels provide an excellent fluid surface area to volume ratio, which allows the reactants to attach to catalyst active sites more quickly.

If used to drive an exothermic combustion reaction using a simple fuel such as hydrogen, a micro-channel reactor can also be used as a very compact heater. Extensive work has been done on catalytic combustion of hydrogen in micro-channel reactors at Oregon State University by Haley and Ghazvini [1] [2]. Haley focused on the development of an experimental unit cell (single channel) micro-reactor with an integrated heat exchanger for use in hydrogen storage applications. Research done by Ghazvini built upon the work done by Haley and developed a multi-channel reactor/heat exchanger for cryogenic hydrogen storage. Ghazvini has also developed a methane-fueled version of the catalytic combustor technology for generating electricity in conjunction with a thermoelectric generator. In all applications of microchannel catalytic combustion, the completeness of

the combustion is directly related to the overall efficiency and environmental cleanliness of the reactor.

High catalyst residence times (defined as the catalyst length over the gas velocity) are typically required to achieve complete combustion, which necessitate either long catalyst sections or low velocity gas. In order to shorten the time required for the hydrogen to mix adequately with air and reach active catalyst sites, pin fins may be used to generate a turbulent flow pattern that may prove highly conducive to mixing.

The objective of this work is to develop a comprehensive framework to quantitatively assess the effect of a MPFA on the hydrogen conversion performance over a plain rectangular channel microreactor.

Two primary performance parameters will be used to assess the effectiveness of the MPFA at various flow conditions: the hydrogen conversion rate and the spatial temperature distribution in the catalyst bed. The hydrogen conversion rate compares the amount of uncombusted hydrogen left in the exhaust gas to the amount that was fed into the reactor. The composition of the exhaust gas is measured using a gas chromatograph, a device that differentiates gas species by their thermal conductivity.

The temperature distribution in the catalyst bed can be used to determine how the MPFA influences mixing directly. Hot spots signify higher reactions rates, which can be used to assess the region of maximum flow residence times. The fluid mechanics responsible for better hydrogen conversion can then be deliberately integrated into subsequent reactor designs. The temperature distribution will be measured directly using an infrared camera. Viewing of the channel is done using a window that seals the gaseous mixture inside the

test section while being transparent to infrared radiation. Non-uniform distribution of the catalyst around the pin fins can cause erroneous temperature profiles, as higher densities of catalyst produce higher temperatures. To account for this, Energy Dispersive X-ray Spectroscopy (EDAX) will be employed to measure the relative amount of catalyst at various spatial locations around a pin of interest. The temperature data will be compared against this distribution to determine if it had a significant impact on the results. The morphology of the catalyst will also be examined using the Scanning Electron Microscope (SEM) that is integrated with the EDAX device.

2 Literature Review

2.1 Pin Fin Flow Mixing Enhancement

To maximize the conversion of hydrogen, the fuel must be mixed as thoroughly as possible with the oxidizing air to maximize combustion rates. A MPFA induces turbulence in the flow, which generates many small vortices that improve mixing. As the incoming flow reaches a row of pins, it must divert around the obstructions. The flow stagnates on the leading edge of the pin, causing high local residence times that increase hydrogen conversion rates. Boundary layers form along the pin walls, which eventually separate as they reaches the opposite side of the row. The separating boundary layers generate turbulent wake regions behind the pins, where unsteady vortex shedding and mixing occur.

As the wake interacts with subsequent pins in the array downstream, additional mixing occurs and conversion of hydrogen asymptotically approaches unity for a long MPFA. Turbulent mixing in the second row of pins is comparatively much stronger than in the first row due to the unsteady vortex shedding according to Ames [4]. An increase in heat transfer of 30-70% was measured in downstream rows compared to that of the first row by Zukauskas [5]. Zukauskas also reported that the heat transfer reached a fully developed value by the third row of pins, indicating that the flow pattern had also reached a fully developed state between subsequent rows of pins. However, other experiments performed by Metzger et al. indicated that the heat transfer rate reached a maximum near the third row of pins and steadily declined in subsequent rows [6].

An increase of up to 10% conversion efficiency was achieved by using pin fins instead of a plain square channel micro-reactor in catalytic methanol steam reforming by Dequing et al. [7].

Unfavorable conversion rates in the reverse Haber process were measured using a catalytic pin fin micro-reactor when compared to the performance of plain square channels by Zheng [8]. However, Zheng attributes the notable differences in conversion rates between the two reactor configurations to variance in the processes used to fabricate the catalyst support. Discrepancies in the anodized surface finish lead to a lower catalyst loading in the MPFA configuration, artificially decreasing the ammonia conversion rate. EDAX will be used to account for the effect of uneven catalyst distribution in this work.

2.2 Catalytic Reaction Investigation Using Infrared Camera

Infrared cameras operate on the principle of Planck's Law, which dictates that a body emits radiation at specific intensities and wavelengths that relate directly to its absolute temperature [9]. IR cameras are able to detect radiation within a discrete band of wavelengths to calculate the absolute temperature of the emitting surface. The quantity of radiation emitted from a black body I^b, or a body that absorbs and emits radiation at all wavelengths, can be expressed as in Equation (1).

$$I^b = \frac{C_1}{\lambda^5(e^{C_2/\lambda T} - 1)} \tag{1}$$

Where λ is the radiation wavelength in meters, T is the absolute temperature of the body in K, and C_1 and C_2 are the so-called first and second universal radiation constants with

respective values of $3.7418 \times 10^{-16}\, Wm^2$ and $1.4388 \times 10^{-2}\, mK$. Corrections to the ideal black body version of Planck's Law can be made to account for the non-ideal emissivity characteristics of a real surface.

In order to obtain meaningful spatially-resolved temperature data from an infrared camera, the radiation sensor must be meticulously calibrated at each pixel of the detector for each test setup. Several factors can cause systematic error in the temperature data if not properly accounted for. Of particular importance are the emissivity of the surface to be measured, background radiation from the ambient atmosphere, and the transmissivity of the test section window. The magnitude of the irradiation detected by the camera I' is described in Equation (2) by Carlomagno and Cardone [10].

$$I' = \tau_t \varepsilon I^b_{obj} + \tau_t (1-\varepsilon) I^b_{amb} + (1-\tau_t) I^b_{atm} \tag{2}$$

Where τ_t is the transmissivity of the medium between the surface and the camera, I^b_{obj} is the radiation intensity corresponding to a black body at the object temperature, I^b_{amb} is the black body radiation intensity corresponding to the temperature of the object surroundings and I^b_{atm} is the radiation intensity corresponding to a black body at the temperature of the atmosphere. The transmissivity of the atmosphere is generally assumed to be unity, which allows for combination of Equation (2) with Planck's law to form a general semi-empirical calibration function for an IR camera given in Equation (3) developed by Carlomagno and Cardone [10]

$$I' = \frac{\varepsilon R}{e^{\frac{B}{T_{obj}}} - F} + (1-\varepsilon)\frac{R}{e^{\frac{B}{T_{amb}}} - F} \tag{3}$$

where R, B, and F are calibration constants that depend on the wavelength of the detected radiation and the camera shutter speed. The calibration of IR cameras using this relationship is very time consuming and necessitates measurement of both the object temperature and the ambient temperature for multiple flow conditions. Instead, a more practical method of in-situ calibration was investigated.

In-situ calibration of infrared camera systems was performed successfully by Sargent et al. and Westby [11] [12]. Sargent used a spatially distributed array of thermocouples attached to a test article to calibrate an IR camera as pictures were taken during an experiment. Westby used one thermocouple to measure the bulk temperature of the test article at various temperatures prior to experimentation. If a constant heat flux is applied to the test section for a long time, the spatial temperature distribution will be nearly uniform if the thermal conductivity of the material is high. With this assumption, data obtained from the IR camera can be calibrated accurately to match the temperature reading from the thermocouple even if the surface emissivity and optical parameters of the test section window vary spatially.

Infrared thermal imaging has been performed on other catalytic hydrogen combustion reactors, most notably by Wonyoung et al. [13]. In their experiments, a NEC Sanei TH9100 infrared camera was used that is able to detect within a bandwidth of 8-14 μm. A Gallium arsenide window was used that is opaque to visible light, but transmits 55% of the 8-14 μm wavelengths. A Jenoptik Vario-Cam HiRes infrared camera with a 640 × 480 pixel detector was used in conjunction with a Fresnel Technologies POLY IR® viewing window to visualize the reaction of a hydrogen/oxygen mixture on a platinum catalyst by Das et al. [14].

2.3 Catalyst Deposition Techniques

To mount a noble metal catalyst in a manner suitable for combustion in microchannels, it must be deposited onto a stainless steel substrate. A wet deposition method was used by Haley and Ghazvini [1] [2] to bond Platinum onto an electrochemically etched stainless steel surface. The noble metal catalyst is dissolved in an appropriate liquid to form a solution. A Kapton tape mask is applied to the support material to contain the catalyst solution in the desired area. A measured amount of the solution is placed in a syringe to obtain the desired catalyst density over the channel area. The solution is carefully applied on the target area and allowed to dry in a warm oven. The deposition and drying process is repeated until all of the measured solution has been used. The downside to the wet deposition method is the uneven distribution of noble metal on the stainless steel surface due to the tendency of the liquid to form droplets as it dries.

A wet impregnation method was used by [15] and [16] to support a Palladium catalyst for combustion of methane. A support material such as alumina is added to provide a porous surface for the Pd. The alumina support increases the number of active sites in the catalyst and helps it adhere to the stainless steel substrate. Palladium precursor compound and gamma phase alumina powder were combined with a solvent and mixed thoroughly with a magnetic stirrer. The liquid is then evaporated and the catalyst is activated via calcining.

3 Measurement Techniques

3.1 Infrared Thermography

To characterize the temperature distribution within the catalyst and hopefully visualize the fluid mechanics associated with the MPFA, an infrared camera will be employed. A high magnification lens will focus on a single pin in the array to visualize temperatures in a local region. In order to obtain meaningful data from an infrared camera, it must be meticulously calibrated to account for the emissivity of the channel surface. Ideally, each pixel in the field of view of the detector would be calibrated individually as the surface is very non-uniform so emissivity can vary substantially even on short length scales. To do this, the test section will be heated for a long time at a constant heat flux to reach a near-uniform surface temperature. Once the channel surface is nearly isothermal, the temperature will be measured using the body temperature thermocouple positioned just behind the channel wall. Due to the reasonably high thermal conductivity of stainless steel, the temperature at the thermocouple and the temperature of the channel are assumed to be identical. The error caused by this assumption is discussed in Section 4.5. While the test section remains isothermal, an infrared picture is taken with the camera emissivity set to 1. This procedure is repeated at multiple temperatures over the expected experimental range to generate a calibration curve for each pixel of the camera detector. Images taken during actual tests are post-processed by fitting a third order polynomial to the calibration data and plugging in the measured temperature from each pixel of the test pictures to generate an image with meaningful temperature data.

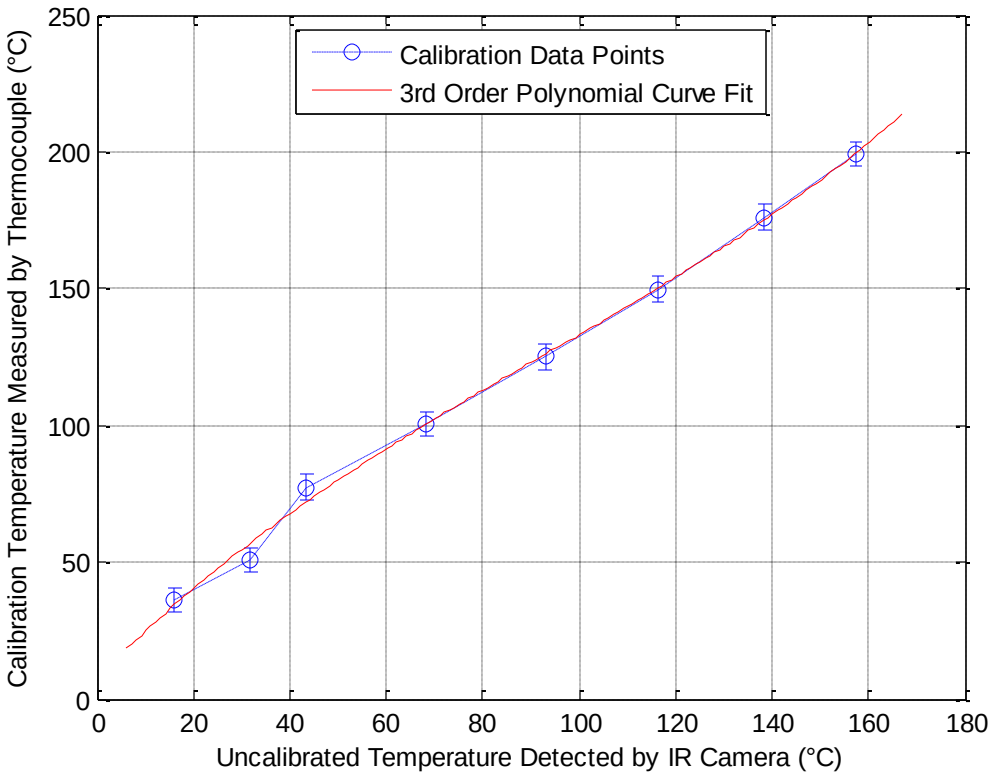

Figure 1 - Example of Single Pixel Calibration Curve from Plain Square Channel with Error Introduced Due to Thermocouple-Channel Surface Gap

A polynomial curve fit was chosen over an interpolation technique in order to extrapolate, as some of the temperatures measured by the infrared camera may be outside of the range of available calibration data. The polynomials demonstrated reasonable extrapolation in regions within 10 °C of the upper and lower extremes of the calibration data.

3.2 Scanning Electron Microscopy (SEM) and Energy Dispersive X-Ray Spectroscopy (EDAX)

In order to isolate the effect of the fluid mechanics of pin fins on hydrogen conversion rates, the spatial variation of catalyst distribution on the channel surface must be accounted. The morphology of the surface can be visually assessed using a SEM. EDAX can be used to measure the weight percentage of discrete chemical elements in a target area determined by the field of view of the SEM. In a ground state, an atom contains electrons in discrete energy levels or valence shells. When the electron beam from the SEM causes a low energy electron to be ejected from the atom, an electron from a higher energy valence shell will take its place. The energy lost from valence shell transition is emitted as an x-ray that is characteristic of the difference in energy and the atomic structure of the emitting atom. The EDAX sensor counts each x-ray and computes the relative abundance of each element in the target area. The same pin examined using infrared thermography is characterized using the EDAX analysis.

3.3 Gas Chromatography

A Gas Chromatograph (GC) is used to measure the chemical composition of the exhaust gasses at various operating conditions. The GC measures the overall performance of the MPFA as opposed to focusing on a single pin fin as in the IR and EDAX analysis. The GC works by mixing the sample with an inert carrier gas (Helium) and injecting the mixture into a glass column coated with a porous material. Larger molecules take longer to diffuse through the material, so gasses of varying molecular weights can be separated

and measured. The GC is calibrated using a mixture of diatomic hydrogen and nitrogen at known concentrations. The output of the calibration gas is compared to the output of an exhaust sample to determine the concentration of hydrogen. The quantity of unreacted hydrogen in the sample is compared to the amount originally introduced into the combustor to calculate the amount of hydrogen that combusted.

4 Experimental Facility and Methods

4.1 Design Requirements

In order to measure the effect of MPFA on catalytic combustion using the techniques explained in Section 3, the experimental facility must meet several requirements.

- Two test section pieces must be fabricated: one for catalyst activation at high temperatures and another for mounting the infrared transparent material for use at lower temperatures.
- The catalyst activation setup must be able to tolerate sustained temperatures of 500 °C.
- A thermocouple must be mounted very close to the underside surface of the test section for accurate calibration of the infrared camera.
- The test section must be mounted in an orientation that allows for easy and consistent camera positioning.
- The test section must integrate into the existing flow loop and be easily removable so that other experiments can be conducted using the same equipment.

The test section was designed and fabricated to meet these requirements. It integrates seamlessly into the existing flow loop, which is detailed in Section 4.2.1.

The results of the experiments will be used to characterize the performance of the square channel and pin fins quantitatively using hydrogen conversion rates and quantitatively using infrared pictures. In order to obtain these performance parameters under various operating conditions, the following measurements were needed:

- Inlet and outlet temperatures of air/hydrogen mixture
- Temperature of the test section channel surface
- Flow rates of air and hydrogen
- The exhaust gas composition
- Pressure drop through the test section

The thermo-fluidic principles that these experiments seek to investigate are:

1. Determination of the effect of pin fin arrays in a catalytic reacting flow, specifically their effect on hydrogen conversion rate and pressure drop.
2. Characterization of the temperature profiles through individual pins to verify enhanced flow mixing or increased local residence times.

4.2 Experimental Facility

4.2.1 Test Section and Existing Flow Loop

The test section for analyzing the performance of a MPFA was fabricated according to the design requirements. A circular configuration was chosen to allow for easy use of high temperature O-rings to seal an existing infrared transparent window made of silicon. Silicon is partially transparent (~55%) to shortwave radiation in the 1.06 to 6.7 μm wavelengths. Stainless steel was chosen as the primary construction material to tolerate the sustained temperatures of steady state combustion. Different catalyst geometries including a square channel, large pin fins (1 mm diameter), and small pins fins (0.5 mm diameter) were etched into stainless steel shims. These shims are interchangeable in the test section depending on which setup needed to be tested. The shim is surrounded by two

stainless steel plates, with one half containing inlet and outlet ports, a thermocouple port, and a cartridge heater port. Two versions of the opposite half were made: one with an opening for an IR transparent window and one without. The piece with no window was used to activate the catalyst, which requires higher temperatures than the window O-ring material can withstand. An exploded view of the test section is shown in Figure 2.

Table 1 - Bill of Materials for Test Section

Part Number	Part Description	Quantity
1	Washer	10
2	Bolt	10
3	Window Plate	1
4	Catalyst Shim	1
5	Silicon Window	1
6	Channel Shim	1
7	Header Plate	1
8	Thermocouple Port	1
9	Nut	10
10	Gas I/O Port	2

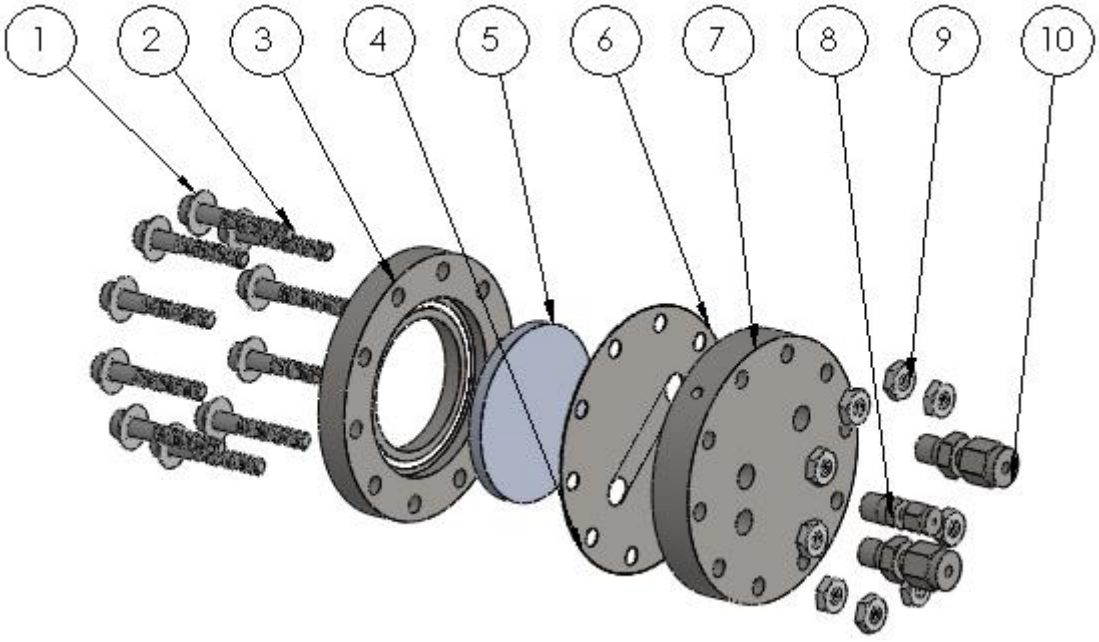

Figure 2 - Exploded View of Test Section Configured for IR Camera Photography

The numbers in each callout correspond to the descriptions and quantities used to construct the test section detailed in Table 1. The fully assembled test section is depicted in Figure 3.

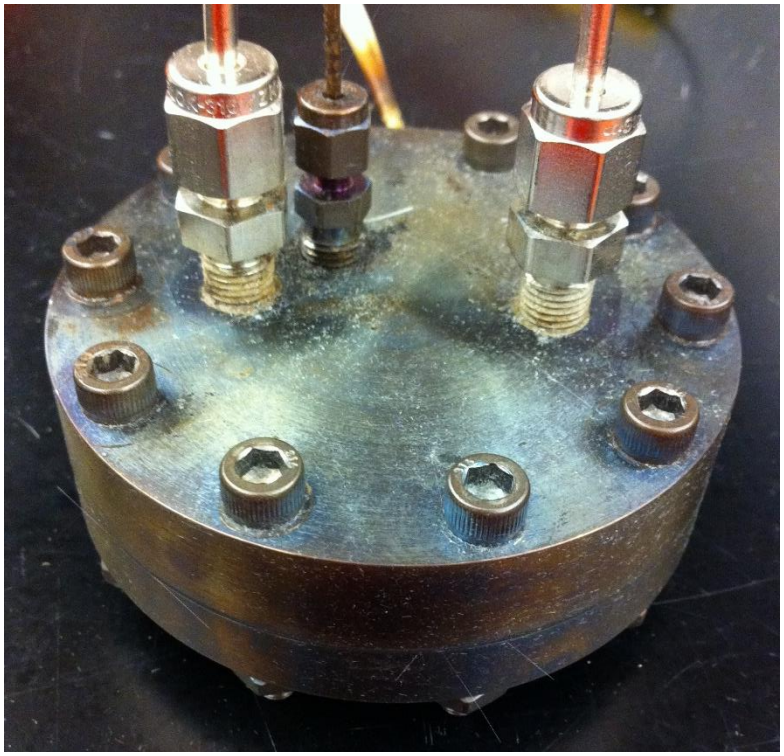

Figure 3 - Assembled Test Section in Catalyst Activation Configuration

The experimental facility used by Haley [1] and Ghazvini [2] in their experiments was adapted for use with the MPFA test section. The entire setup is contained under a fume hood that supplies air, nitrogen, hydrogen, and cold water to the flow loop. The flow loop contains various valves and sensors that measure and control the test section inlet conditions. Air and nitrogen supplies are regulated to 3.5 bar (~50 psi), while hydrogen is regulated to 20 psi. Nitrogen is used during the calcining process and to purge the flow loop after testing with hydrogen to ensure safe shutdown. During testing, the flow rates of air and hydrogen are controlled separately using two parallel mass flow controllers

(MFCs). Safety devices called flashback arrestors close off the air and hydrogen supplies in the unlikely event of uncontrolled flame propagation upstream from the test section.

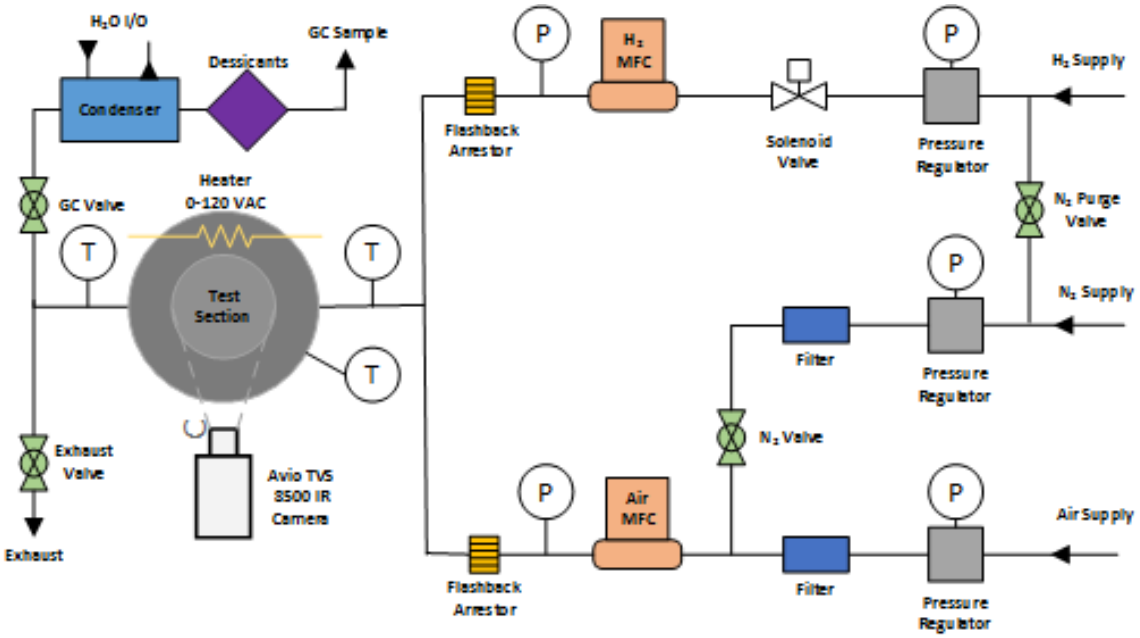

Figure 4 - Experimental Facility Schematic

The test section is instrumented with a single T-type thermocouple, which is used to calibrate the infrared camera. During normal operation, the combustion products are continually exhausted into the fume hood. Even if there is no combustion occurring, the hydrogen/air mixture is dilute enough so that never exceeds the lower flammability limit to ensure safety. In order to take a sample of the exhaust gasses for GC analysis, the exhaust valve is closed and the flow is diverted through a condenser to eliminate the majority of water vapor contained in the exhaust. The remaining water vapor is eliminated by feeding the gas through two desiccants and into sample bags for analysis.

4.2.2 Catalyst Shims

A plain square channel was manufactured using an inexpensive laser cutting technique. Two separate shims were cut out of 203 µm stainless steel shim stock, one with the channel geometry cut away and one with no channel geometry. The shim with the channel geometry was used as a spacer to create the channel between the two halves of the test section. The channel is depicted with detailed dimensions shown in Figure 5.

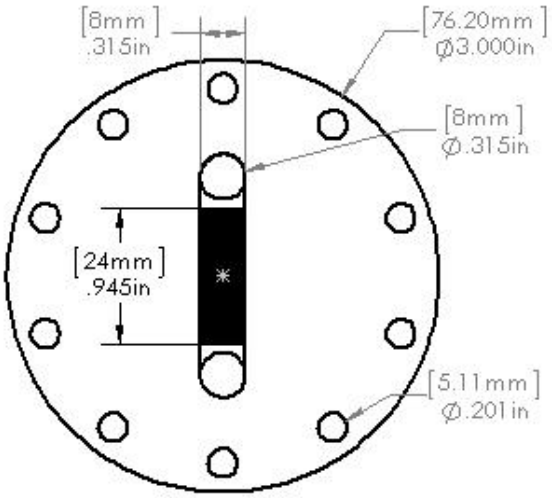

Figure 5 - Straight Channel Shim for Control Experiment

The pin fin channels could not be laser cut as with the plain square channel, so they were constructed using a chemical etching process. The geometries of the 0.5 mm and 1 mm pin fin channels are depicted in Figure 6 below.

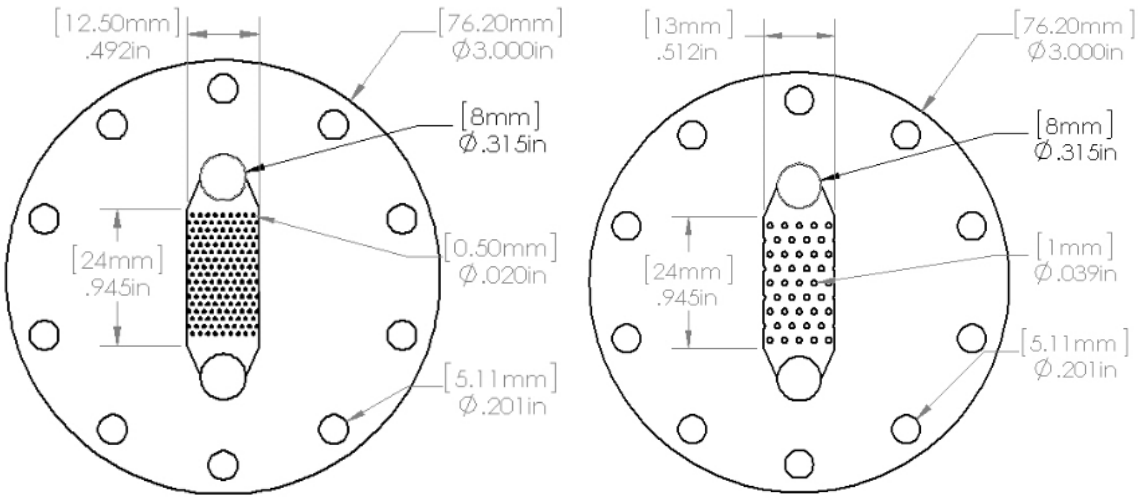

Figure 6 – a) 0.5 mm MPFA Shim b) 1 mm MPFA Shim

The channels are designed such that the wetted cross sectional area of all three shims is equivalent. The MPFA shims have much wider channels since the pin fins take up a significant portion of the channel area.

4.2.3 Infrared Camera

The infrared camera used in experimentation is an Avio TVS-8500 (CMC Electronics), which has a temperature range of 20°C to 300°C and a field of view of 2.56 x 2.36 mm using a TVL-8510U lens. The lens can achieve a 10 µm resolution using a 256 x 256 pixel detector at a fixed focal length of 27 mm. The camera is sensitive to infrared emissions in the 3.5 to 4.1 µm and 4.5 to 5.1 µm range, which matches well with the transmission wavelengths of the silicon window.

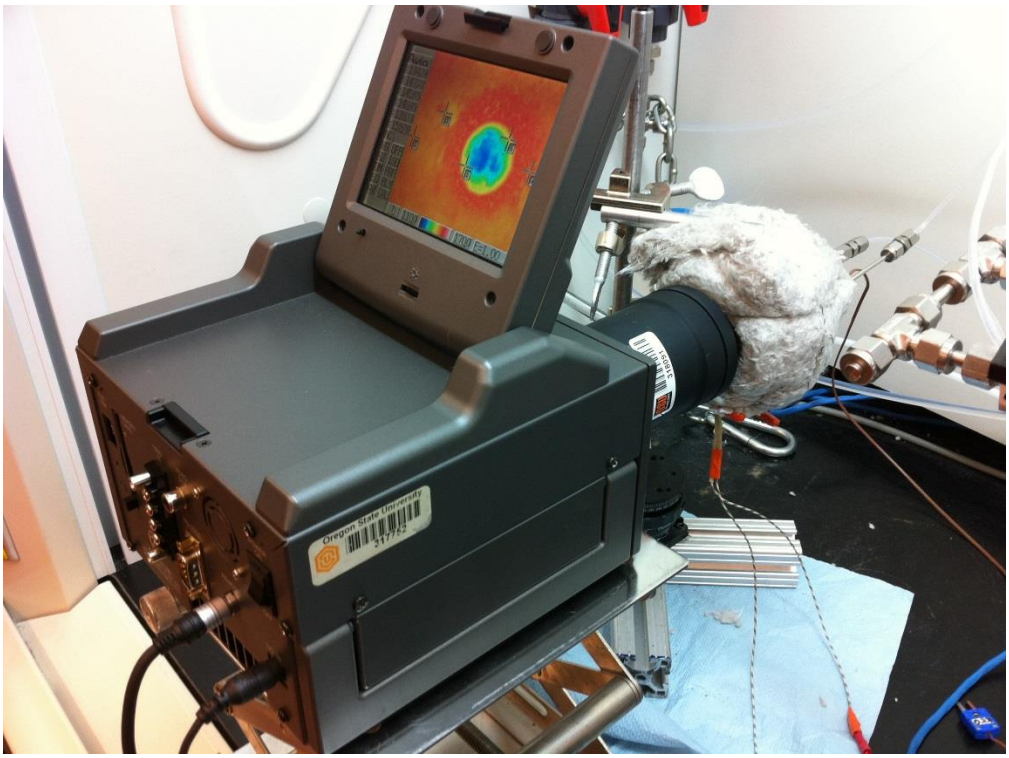

Figure 7 - Avio TVS-8500 Infrared Camera in Testing Configuration

Care must be taken to orient the camera so that the lens is normal to the channel surface. If there is a significant angle between the two, the directional emissivity of the material will give false temperature readings [17]. It is important to position the camera consistently for each test to avoid image post processing to account for different camera orientations.

4.3 Catalyst Preparation and Activation

Significant work must be done to securely attach the catalyst material to the channel surface. The procedures required to ensure proper adhesion to the channel are described below.

4.3.1 Catalyst Preparation

A platinum salt solution was wet deposited on the surface of the channel using the process developed by Stefanov et al. [18].The Platinum precursor compound Chloroplatinic acid hexahydrate ($H_2PtCl_6 \cdot 6H_2O$) with a purity in excess of 95% was obtained from Sigma-Aldrich®. The molecular weight of the compound is 517.90 g/mol. A 0.007 M solution of the acid was made using deionized water. Then small syringes of precisely measured volumes of solution were used to deposit the solution on the stainless etched catalyst shims. The amount of acid required to create sufficient active sites for reactions to occur was determined by multiplying the surface area of the channel by a loading density of 0.529 ml/cm^2. The solution had to be carefully dripped onto the shim in several steps, as there was too much liquid to apply all at once. After each application of acid on the surface, the shim was allowed to dry in a warm oven before carefully depositing another layer.

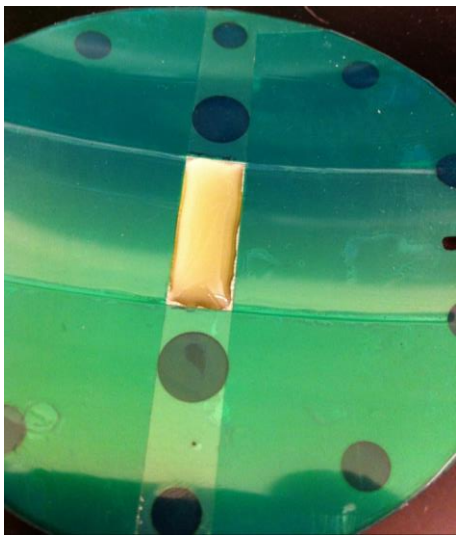

Figure 8 - First Round of Wet Deposition on Test Shim

A mask of RTV silicone rubber was used to prevent the acid from flowing out of the target region while it evaporated. As the acid is heated during the catalyst activation procedure, the following reaction steps occurred and it decomposed first into platinum chloride and then into elemental platinum [19].

$$(H_3O)_2PtCl_6 \cdot nH_2O \leftrightarrow PtCl_4 + 2HCl + (n+2)H_2O \quad (4)$$

$$PtCl_4 \leftrightarrow PtCl_2 + Cl_2 \quad (5)$$

$$PtCl_2 \leftrightarrow Pt + Cl_2 \quad (6)$$

4.3.2 Chemical Etching

Prior to depositing the catalyst onto the stainless steel shim, the target area must be electrochemically etched in order to increase the surface roughness and porosity. This allows the catalyst to adhere to the steel much more effectively. Etching was performed using a 0.5M aqueous oxalic acid solution as described by Stefanov et al. [18]. The stainless steel shim was masked with Kapton tape to prevent etching in the non-target regions. Small cutouts were made in the masking tape to allow alligator clips to have good electrical contact on the metal. The target region was immersed in the oxalic acid solution parallel to a submerged sacrificial steel plate.

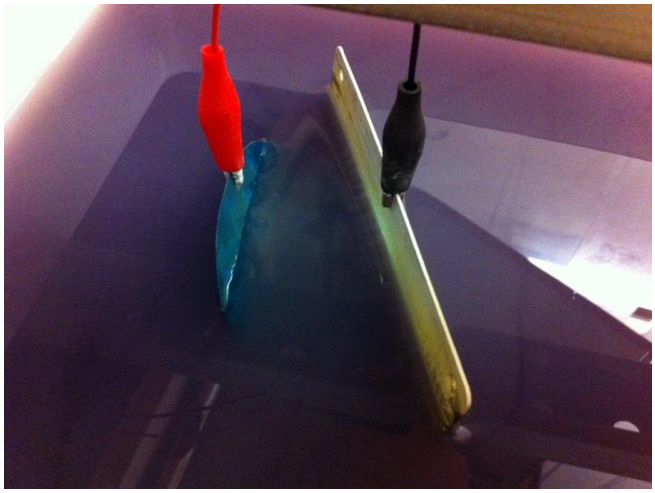

Figure 9 - Electrochemical Etching Setup

With the shim to be etched as the anode and the sacrificial plate as the cathode, a voltage is applied such that the current density on the target area is 0.28 A/cm^2. In practice, this resulted in applying sufficient voltage to drive approximately 0.5-0.8 amps of current through the shim. Significant amounts of waste material would build up on the sacrificial plate, requiring removal with a razor blade between etching runs. The acid solution was saved after each procedure and reused repeatedly with good results.

4.3.3 Catalyst Activation

In order to remove the water trapped in the dried catalyst, the shim is heated while allowing inert nitrogen gas to flow over it. This procedure is known as calcining and produces the reaction described in Equation (4). After the calcining has been completed, the catalyst is then reduced at the same elevated temperature using a 10:1 ratio of nitrogen and hydrogen gas to allow the reactions in Equations (5) and (6) to take place. Common temperatures for calcining and reducing lie between 500°C and 600°C

according to literature [13] [20] [21]. To survive extended periods at these high temperatures, the activation test section was made completely out for stainless steel. For calcining, nitrogen was allowed to flow through the combustor while a cartridge heater raised the temperature of the combustor to 500°C and maintained it for 2 hours. Then a 10:1 volumetric ratio of nitrogen and hydrogen was allowed to flow inside the channel for an additional 4 hours for the reduction step. The heater and hydrogen were shut off and the combustor was allowed to cool down to room temperature while nitrogen continued to flow through the channel.

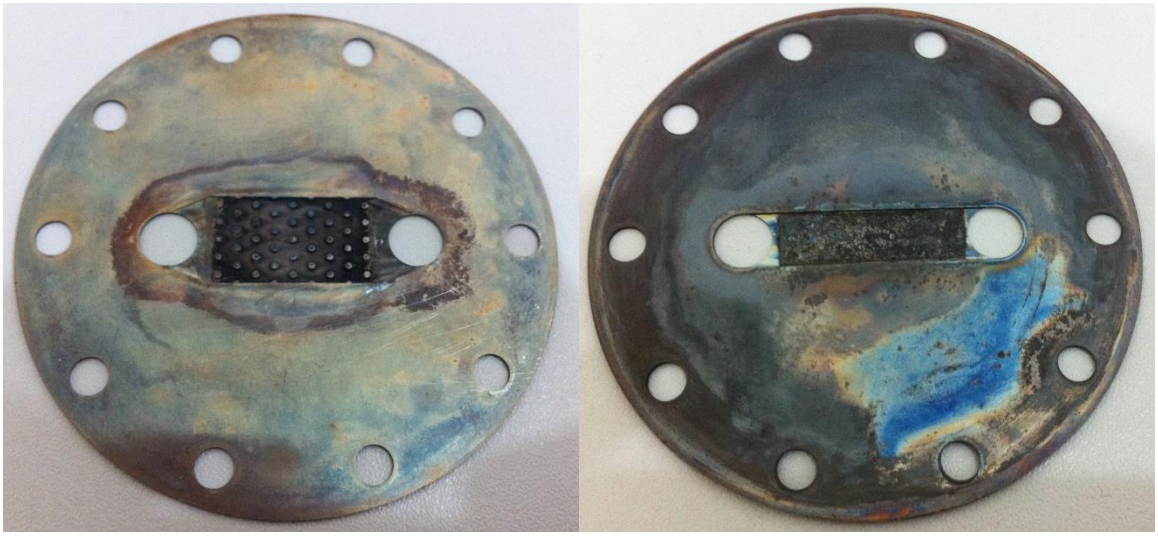

Figure 10 – a) 1 mm MPFA and b) Plain Square Channel Shims after Deposition and Calcining

The shims became discolored due to the high temperatures they experienced during calcining. The catalyst became very black with a slightly flaky texture.

4.4 Experimental Procedures

The infrastructure required to operate the test section is complicated and extensive. The following sections describe the procedures that were developed by Haley and Ghazvini [1] [2] to operate the flow loop equipment.

4.4.1 Startup Procedure

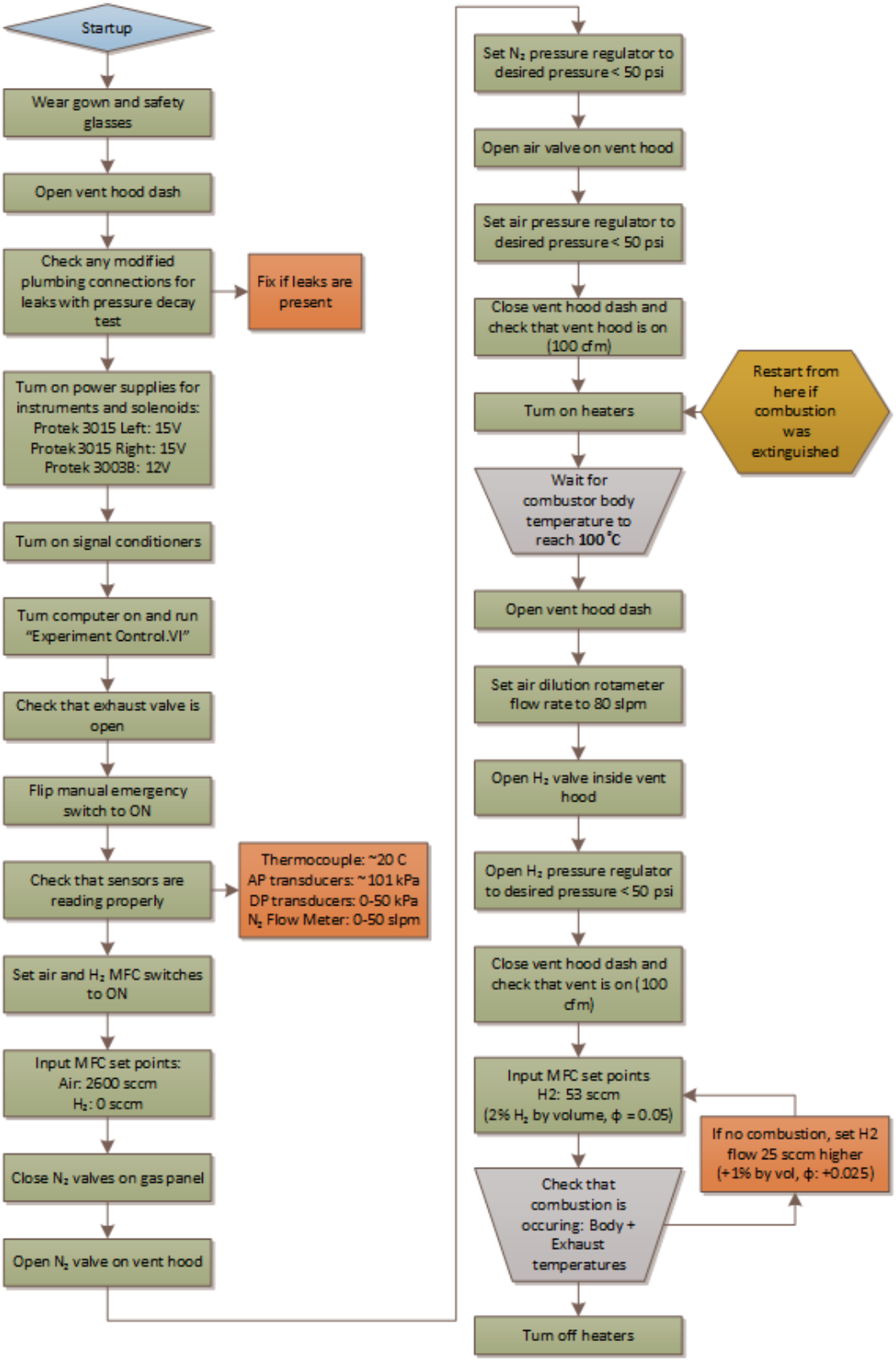

Figure 11 - Startup Procedure

Before starting an experiment, the experimental facility was checked according to the flowchart shown in Figure 12.

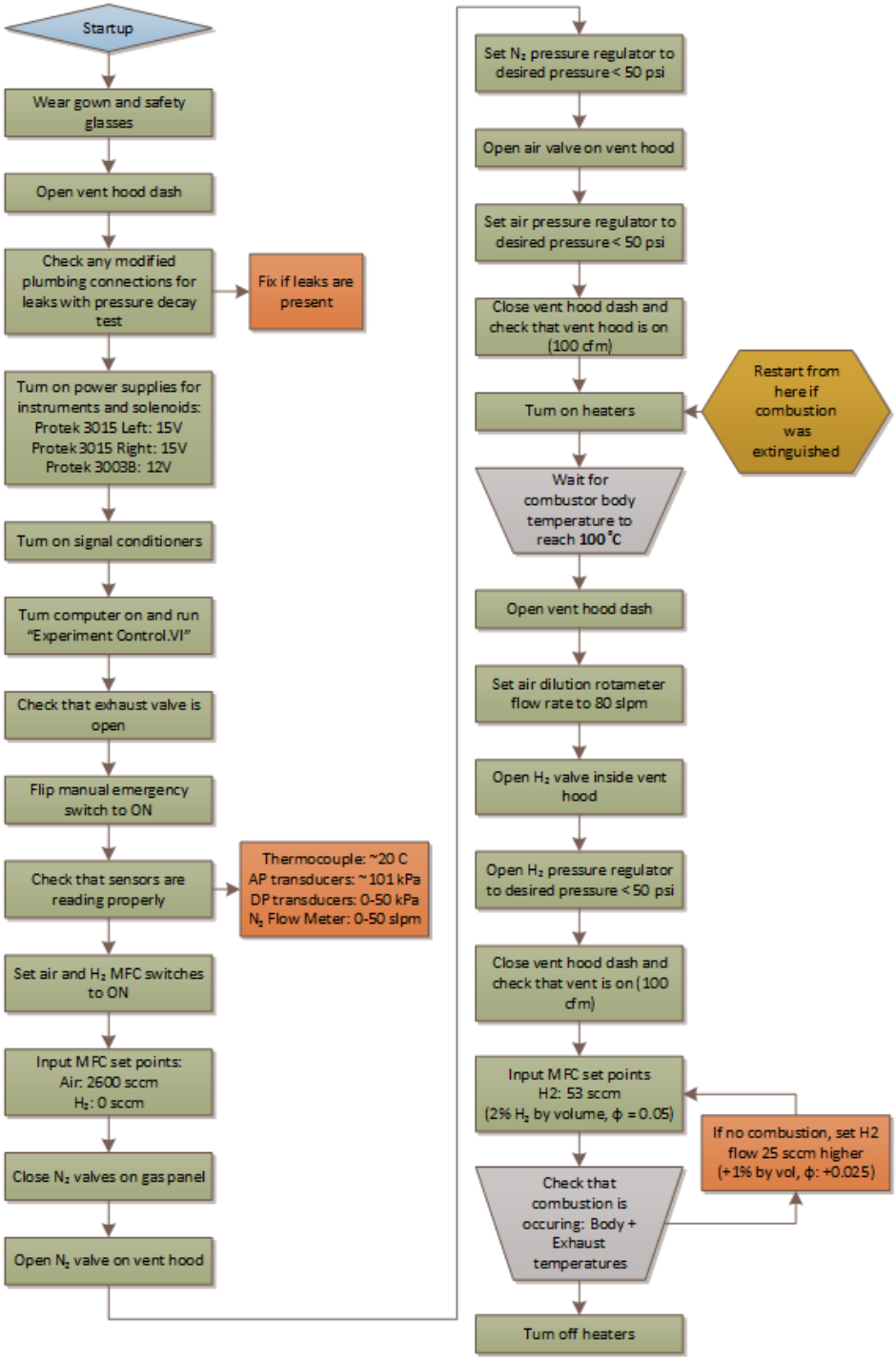

Figure 12 - Startup Procedure

Safety glasses are worn while working within the hood. If any modification has been done on the test section or in the plumbing, they were checked for leaks before starting the experiment. Power supplies for MFC's and pressure transducers were turned on. The desiccants were also checked and make sure that they were not in the active flow loop (the valve was closed).

The desiccants were only in the loop when samples were taken from the exhaust gases. If the color of the desiccant's beads were blue instead of the normal yellow, they were replaced. Once the flow loop was inspected, the LabVIEW program was started. The program starts collecting data immediately, but the data was not saved until the save button was pressed. All temperatures and pressure transducers readings were checked at this point to make sure that all are within the expected range.

With the system check completed, the experiment was started. After the air valve was opened, the rotameter in the exhaust line was adjusted to keep the exhaust gas composition below the flammable range for the worst case that all the hydrogen flowing through the combustor remained unreacted. Preheating the combustor was necessary for the reaction to initiate. A body temperature of about 50 °C was sufficient to start the reaction. The reaction was very slow at those temperatures; therefore in order to save time and reach a steady state sooner, the combustor was preheated to 80 °C -100 °C before letting hydrogen flow within the combustor. At this point data saving was initiated in LabVIEW and the heater was turned on and adjusted using a variable AC voltage supply. The power was slowly increased while a low flow rate of air (1000 sccm) was allowed to flow through the test section. When the desired temperature was reached, the

heater was turned off and unplugged. The air flow rate was increased to 2600 sccm and hydrogen valve was opened. Hydrogen was allowed to flow through the combustor with an equivalence ratio of 0.05. The equivalence ratio was increased until a noticeable increase in the temperature was observed. Body temperature was monitored to ensure that it remained below the maximum allowable temperature (250 °C). If the temperature reached 250 °C, hydrogen solenoid valve and heaters were automatically shut and air flow rate was set to maximum to cool down the test section. Exhaust temperature was also checked continuously by the LabVIEW program to make sure that it remained higher than 100 °C in order to prevent condensation inside the test section.

4.4.2 Continuous Operation

It took between 5 and 30 minutes to reach steady state conditions at desired operating conditions of air/H_2 flow rates, combustion temperature, and equivalence ratio. Steady state condition was defined as the state which the combustor body temperature remained within 0.5 °C for 5 minutes. Upon reading the steady state, the infrared camera was used to take a picture of the channel. If the high magnification lens was being used snapshots would be taken of between 1 and 3 pins. The time that the picture was taken was noted by commenting in the LabVIEW program. At the same time, a gas sample was collected for analysis in the GC. Once the sample was collected, a different flow rate or temperature was tested based on the experimental matrix or the shutdown procedure was initiated.

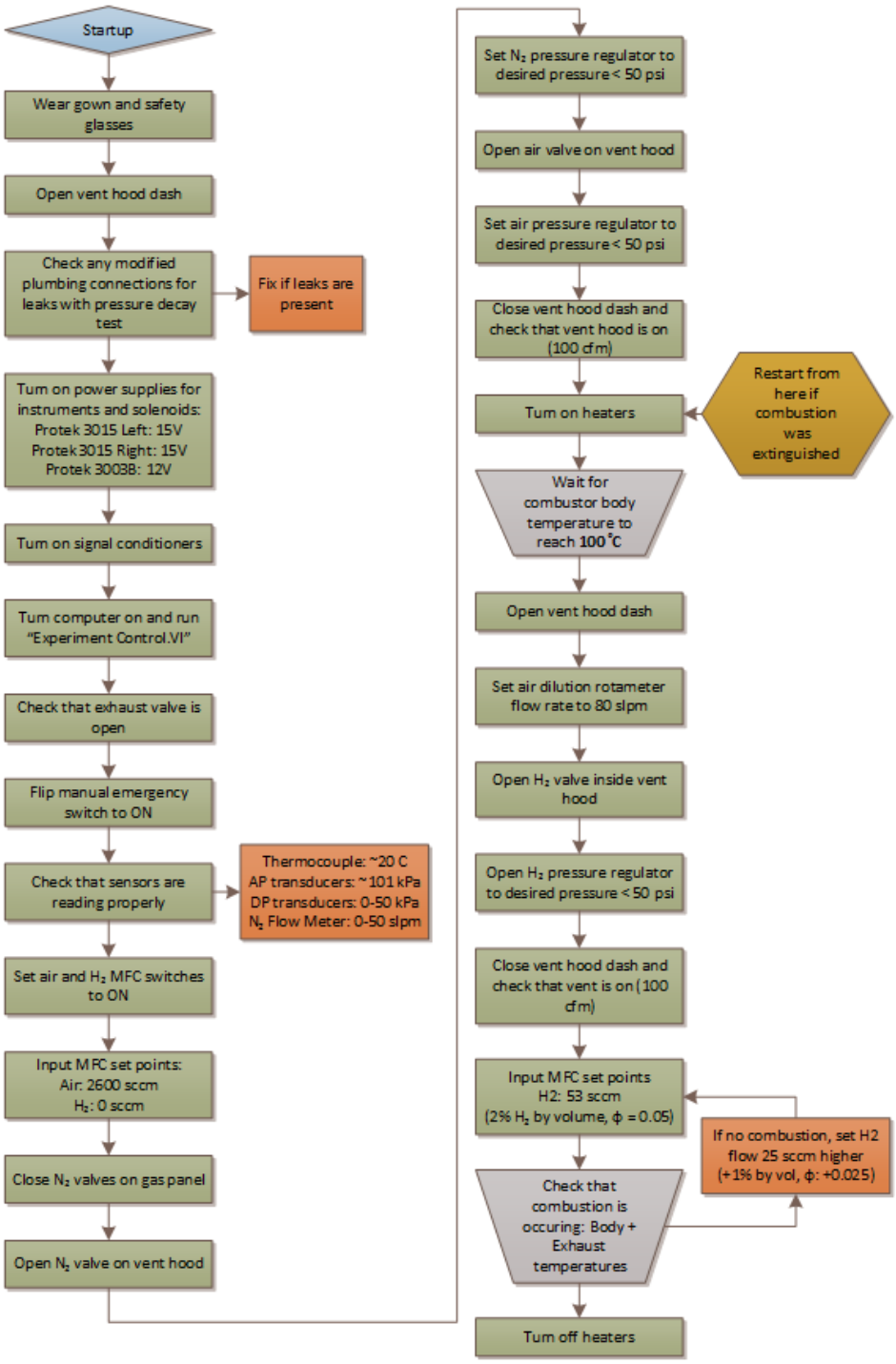

Figure 12 - Startup Procedure

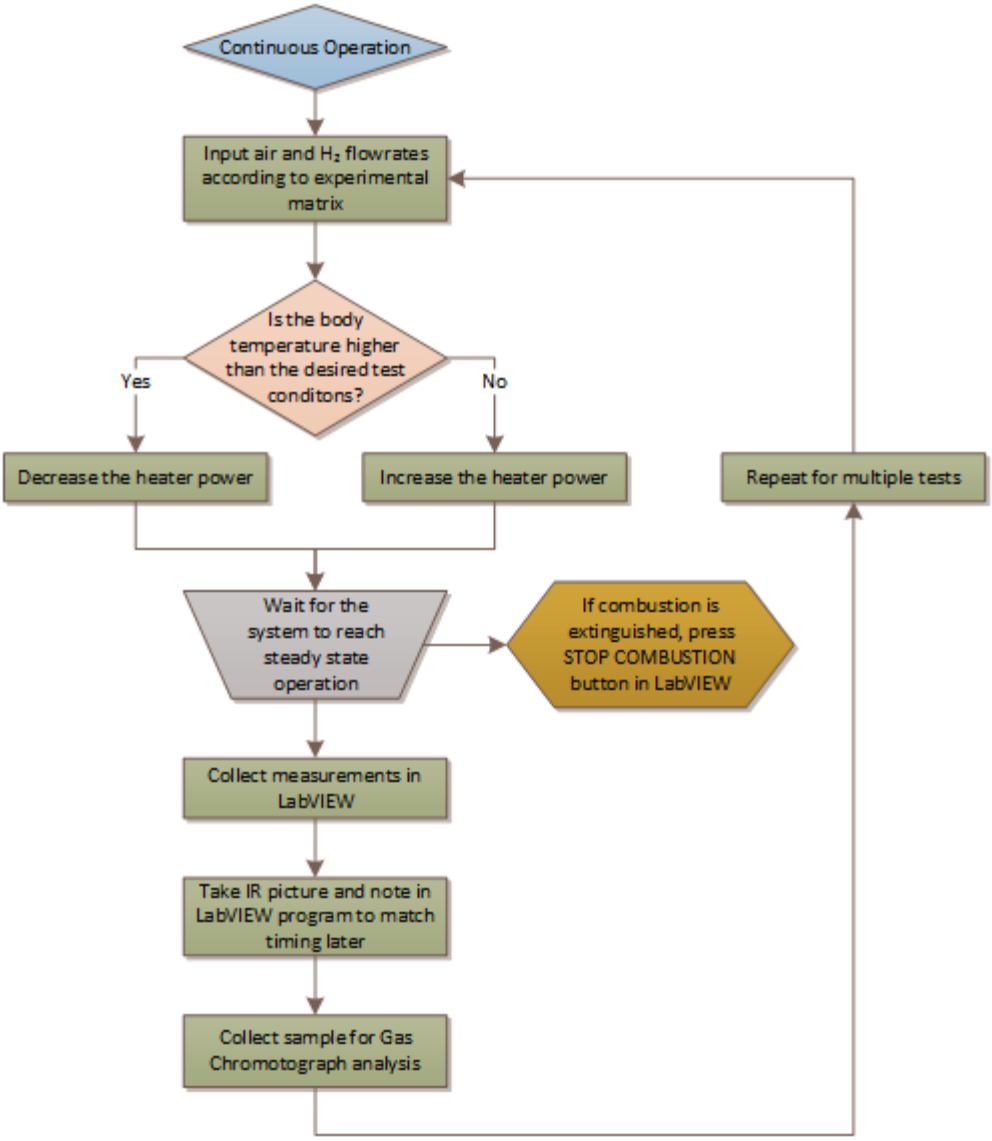

Figure 13 - Continuous Operation Flowchart

4.4.3 Shutdown Procedure

A series of steps were followed in order to safely shutdown the system after all data and samples had been collected. A flow chart of the procedure is shown in Figure 14. The vent hood dash was opened just enough to close the hydrogen main line (regulator). The

hydrogen solenoid valve remained open to empty the remaining hydrogen in the lines through the exhaust line. Once the pressure on the hydrogen regulator dropped to less than 69 kPa (10 psi), the nitrogen valve on the hydrogen line was opened to purge the lines (Figure 4). The outside hydrogen supply was shut off at this time as the combustor is allowed to cool. Once the purge was completed and the body temperature dropped below 50 °C, the air and nitrogen valves were closed and the LabVIEW program was stopped. Finally, all the power supplies were turned off.

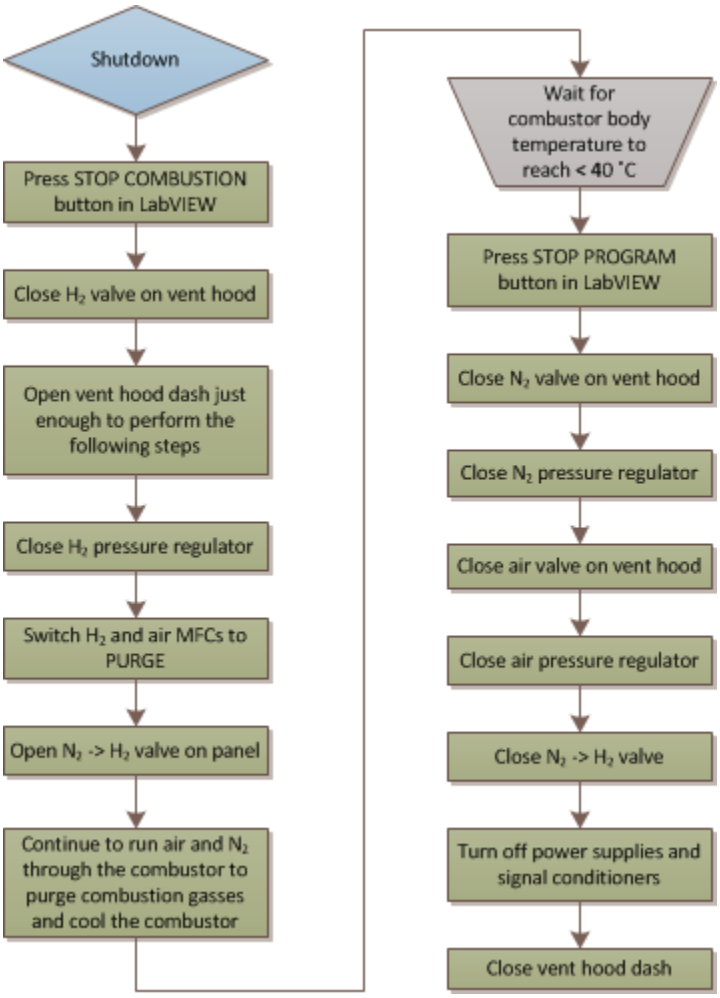

Figure 14 - Shutdown Procedure Flowchart

4.4.4 Emergency Shutdown Procedure

A flow chart was prepared describing the emergency shutdown procedure and is presented in Figure 15. An internal code was programmed in LabVIEW to stop the reaction and thus heat generation with one click. Hydrogen MFC was normally closed and air MFC was normally open therefore, in case of a power outage, air would flow inside the combustor without hydrogen and cool it down.

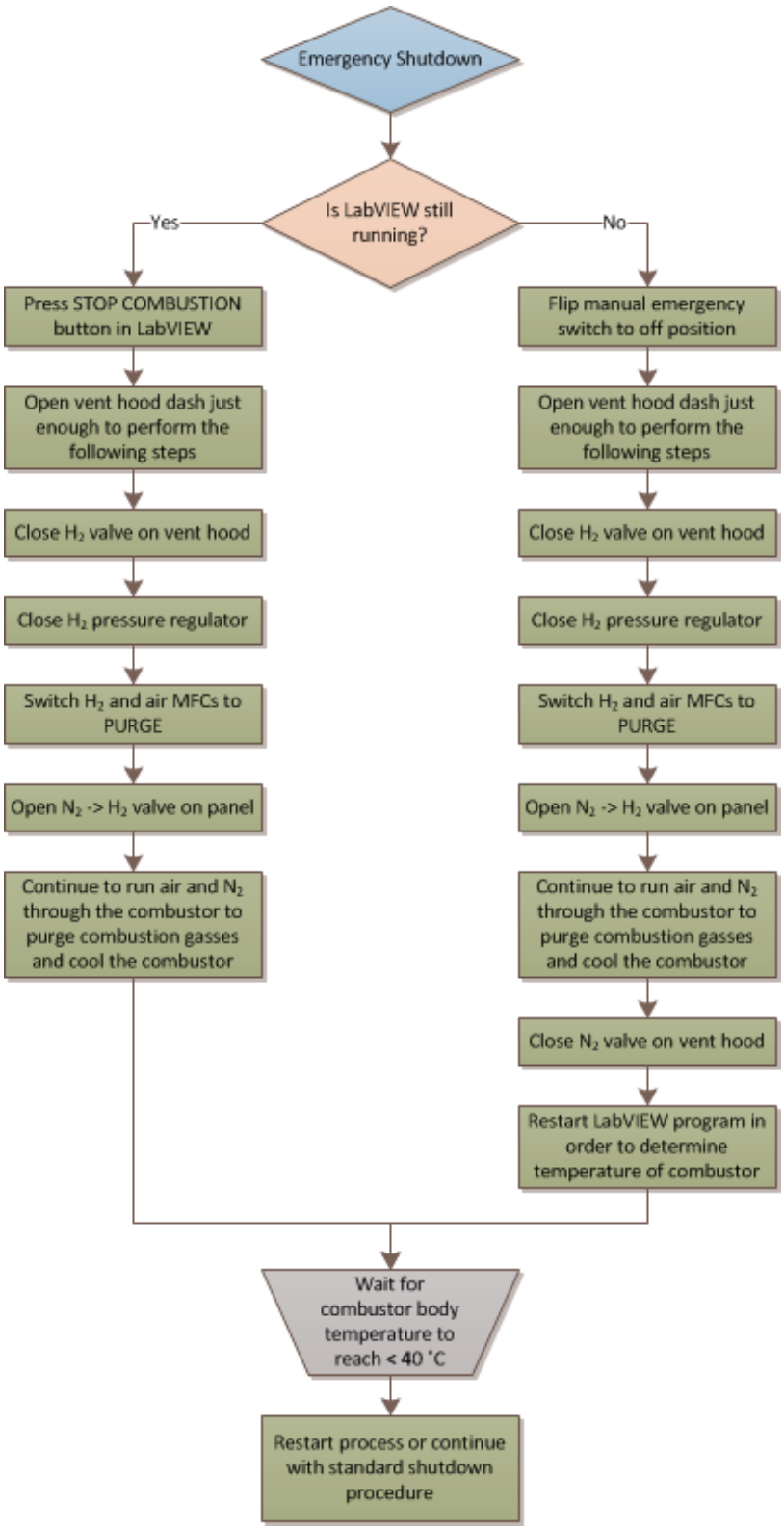

Figure 15 - Emergency Shutdown Procedure

4.4.5 Hydrogen and Methane Supply Operation

Hydrogen supply to the lab was provided by two hydrogen tanks that were contained inside a safety cabinet located outside of the hydrogen storage lab. If one of the cylinders was emptied, the cabinet automatically switches to the other cylinder and alerts the operator to change the empty cylinder. The cabinet is controlled using a touch screen. If the delivery pressure of hydrogen was more than a maximum designated value (80 psi), an alarm would go off and hydrogen shuts down until the pressure is adjusted.

4.4.6 Infrared Camera Operation

The infrared camera described in Section 4.2.3 was used to obtain spatial temperature distribution profiles of the catalytic bed. The camera was positioned on a variable height platform that was adjusted with a lead screw. The high magnification lens was positioned so that the surface of the silicon window was about 24 mm away from the lens and manually adjusted until the surface of the channel was in focus.

The calibration procedure described in Section 3.1 was performed over a range of 8 different temperatures in the range of 25-200°C with an air flow rate of 400 sccm going through the test section. At each of the calibration temperatures, the exact reading of the body thermocouple and the file name of the picture were noted. Once calibration was complete, the same procedure was followed to gather temperature data for each test condition.

4.4.7 Gas Chromatograph Operation and Data Analysis

Samples are taken of the exhaust gas using small bags that are designed to have gas injected with a needle and a valve that allows the GC to suck in the sample. Samples are taken at the same time that infrared images are captured. The bag is taken to the GC and analyzed within 30 minutes of obtaining it. Each sample bag contained enough gas to get three measurements. The spread of these measurements were analyzed to determine the repeatability of the GC.

4.4.8 Catalyst Loading Characterization using a Scanning Electron Microscope (SEM) and Energy Dispersive X-ray Spectroscopy (EDAX)

A series of EDAX measurements were taken around a representative pin in the center of the seventh row from the inlet (indicated in Figure 16) to quantify the uniformity of the platinum loading in that area. This particular pin was selected due to the location in the fully developed region of the MPFA and the visually uniform distribution of catalyst around it. A FEI Quanta 600F SEM with EDAX capability was used to take these measurements. The SEM target area is a square with an edge length of approximately 250 μm at 500X magnification. Measurements were taken at eight points at intervals of 45 degrees, all an equidistant 750 μm from the center (250 μm from the edge) of the pin. Two additional measurements were taken both upstream and downstream of the pin at 1 mm and 1.5 mm from the center for a total of 12 EDAX data points. The locations of the points relative to the pin of interest are depicted in Figure 16.

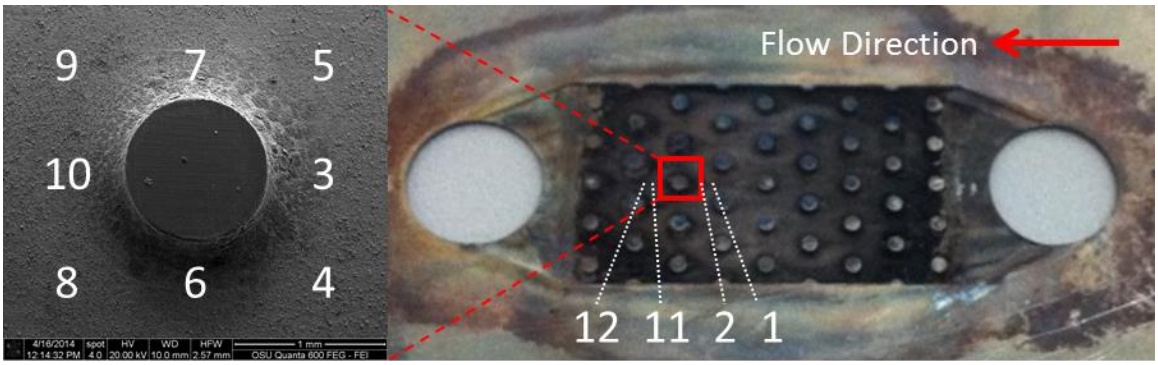

Figure 16 - Location of Pin Used in Detailed EDAX Measurements and Location/Numerical Designation of Target Areas Surrounding the Pin

4.5 Sources of Uncertainty

4.5.1 Spatial Temperature Distribution Measurement Using an Infrared Camera

There are two primary sources of uncertainty associated with measuring the spatial temperature distribution of the catalyst bed. The most obvious cause of temperature uncertainty is the sensitivity of the camera itself. The second source of uncertainty arises from the calibration procedure and encompasses two factors. Sources of error lumped into the camera calibration include the temperature difference between the catalyst and the tip of the body thermocouple, and the error introduced by curve fitting a finite dataset with relatively nonlinear behavior. In order to quantify the effect that these uncertainties have on the final temperature data, the Kline-McClintock method of uncertainty propagation will be used in conjunction with some conservative assumptions for the magnitude of the error.

The sensitivity of the TVS-8500 IR camera is given by the manufacturer as 0.025°C. The maximum possible temperature difference between the catalyst surface and the body thermocouple can be calculated by performing a simple conduction heat transfer calculation according to Equation (7) assuming that the entire heat output of the combustor is applied to a small area of the test section wall.

$$q'' = -k\frac{\Delta T}{\Delta x} \tag{7}$$

Where q'' is the heat flux applied to the channel wall in W/m^2, k is the thermal conductivity of the channel wall in W/m-K, ΔT is the temperature difference across the wall, and Δx is the thickness of the wall. With the thermal conductivity of stainless steel (20 W/m-K), a channel to thermocouple gap of 2.3 mm, and a maximum heat output of 4×10^5 W/m^2, the maximum possible temperature difference between the channel and the thermocouple is 4.6°C. The effect of using an extrapolated curve fit to calculate temperatures will be determined during the propagation of uncertainty step. The total uncertainties are depicted as error bars in the plots in Section 4.4.6.

4.5.2 Exhaust Gas Composition Measurement Using a Gas Chromatograph

The uncertainty associated with the gas chromatograph arises primarily from the lack of good repeatability of exhaust gas composition measurement, even when measuring the same sample multiple times. To account for this, each sample will be analyzed a total of three times in order to calculate the precision uncertainty for each data point. A student-t statistical distribution will then be used to calculate the precision uncertainty, which will be combined with the manufacturer-specified bias uncertainty to calculate a total

uncertainty associated with the measurement of the hydrogen and nitrogen peaks in each sample. The Kline-McClintock method of uncertainty propagation will again be used to derive a total uncertainty for the hydrogen conversion rate. The uncertainty results are depicted as error bars in the tables in Sections 5.3.1.2, 5.3.2.2, and 5.3.3.2.

4.6 Safety Considerations

Note: This section has been adapted from Ghazvini [2] as the majority of the experimental facility and failure modes are identical. It is worthwhile to document the effort put into making operation of the experimental facility as safe as possible, both as a convenience for the reader and to stress the importance of the safety measures put into place as a result of the following analysis.

The facility has been designed for accuracy and safety. The primary safety concern is preventing a flame from propagating upstream to either the hydrogen or air source. Safety measures have been put in place to passively prevent the flame from propagating upstream and to actively suppress the flame should the passive system fail.

Flame arrestors have been placed downstream of the mass flow controllers in the hydrogen and air lines. These are devices that prevent a flame or explosion from propagating upstream to the air or hydrogen sources. There is a sintered material in the arrestor that passively absorbs heat, which stops a flame from moving upstream. There is also an internal check valve that closes in the event of an explosion, preventing the hot gas from flowing back into to the MFC. The valve is automatically reset by supplying

flow in the correct direction. Additional check valves are located on the H2 line, N2 line and air line to prevent back flow of any gases to the gas supply lines or dilution system.

As a backup for the flame arrestors, the H_2 MFC contains a primary normally-closed solenoid valve. A secondary normally-closed solenoid valve is located on the hydrogen line between the MFC and the pressure regulator. The air MFC contains a normally-open solenoid valve. The solenoid valves can be activated by one of four means: (a) an emergency switch within the LabVIEW program, (b) a LabVIEW software trigger controlled by the test section body temperature sensor, (c) a manual switch located near the vent hood, or (d) a loss of power.

Failure modes have been considered using a Failure Modes and Effects Analysis (FMEA). This process is a quantitative way to address failure risk for a product, system or process. The results of this analysis are tabulated in Table 3 and the corresponding legend is shown in Table 2. The failure modes are ranked based on their risk priority number. This value is the product of the severity, occurrence and detection ratings. Failure modes are described in detail in the paragraphs following the tables.

Table 2 - FMEA Legend

Severity Rating (S)	**Meaning**
1	Negligible Effect
2 to 3	Minor
4 to 6	Moderate
7 to 8	High
9 to 10	Very High (Results in unsafe operation)
Occurrence Rating (O)	**Meaning**
1	Essentially Never
2 to 3	Low (few failures)
4 to 6	Moderate (occaisional failures)
7 to 8	High (repeated failures)
9 to 10	Very High (inevitable failure)
Advance Detection Rating (D)	**Meaning**
1	Negligible (certain detection)
2 to 3	Low Risk (easily detected)
4 to 6	Moderate Risk (sometimes detected)
7 to 8	High Risk (unlikely detection)
9 to 10	Very High Risk (impossible to detect)

Table 3 - Failure Modes and Effects Analysis Results

Failure Mode	Effects	Severity Rating (S)	Cause(s)	Occurrence Rating (O)	Current Controls	Advance Detection Rating (D)	Risk Priority Number (RPN)
Flashback	Very high temperatures and fast upstream flame propagation	9	Homogeneous combustion, low flow rate s and high temperatures	2	Flashback arrestors are located before the MFCs. Extreme temperatures will trigger program to extinguish combustion	10	180
Sustained homogeneous combustion in the test section	Very high temperatures. May melt test section if sustained.	5	Low flow rates and high temperatures	4	Extreme temperatures will trigger program to extinguish combustion	2	40
Hydrogen leak in the test section	Fire risk	2	Improperly tightened fittings or test section, IR window O-Ring not sealing	3	Test section is located within a vent hood. Test section tightened with torque wrench and leak tested after every reassembly	5	30
Hydrogen leak in the flow loop	Fire risk	2	Improperly tightened fittings	2	Entire flow loop is located within a vent hood. An alarm goes off if the vent hood fails. H2 lines have been pressure tested to 50 psi.	5	20
Power Failure	Vent hood, computer, and flow controllers turn off	2	City power outage	1	H2 flow is stopped by normally closed solenoid and MFC. Air continues to flow through a normally open MFC.	10	20
Unreacted hydrogen in exhaust	Fire risk	1	Combustion not occurring, low temperatures	2	Entire flow loop is located within a vent hood. The exhaust gas is diluted below flammability limit if combustion was not occurring.	1	2

Flashback: A flashback in the combustor or lines would result in very high temperatures and fast upstream flame propagation. To prevent flashbacks from damaging equipment,

flashback arrestors are located before the MFCs. Flashback arrestors are standard components for welding systems; they have a sintered element that prevents upstream flame propagation and a check valve to prevent backflow. If a flashback has occurred, the LabVIEW program will automatically detect it based on the line temperatures and shut off the H_2 flow. The severity of this failure is expected to be low (S=3) due to the flashback arrestors. The occurrence of this failure is expected to be moderately low (O=4) because the combustor has been designed to be intrinsically safe with channel sizes that should be too small for homogeneous combustion. Based on our current understanding of the system, flashbacks cannot be detected in advance (D=10). This results in a cumulative RPN of 120. While this is higher than preferred, it is acceptable because the severity of the failure is low.

Sustained Homogeneous Combustion in Test Section: Sustained homogeneous combustion (without flashback) in the test section would result in very high temperatures and may melt the test section. To prevent sustained homogeneous combustion, the LabVIEW program will automatically shut off the H_2 flow once a specific combustor body temperature is exceeded. This limit will be 250°C, which is near the melting temperature of the O-ring used to seal the gas inside the silicon window. The severity of this failure is high (S=9) because meltdown of the test section would be very dangerous and costly. The occurrence of this failure is expected to be moderately low (O=4) because the combustor has been designed to be intrinsically safe. This failure will occur only if homogeneous combustion is sustained and it will be easily detectable with the thermocouple attached to the body of the combustor (D=2). This results in a cumulative

RPN of 72. While this is higher than preferred, it is acceptable because it should be detected and easily stopped before it can cause damage.

Hydrogen Leak in Test Section: The entire flow loop is located within a vent hood. Any leaks would be rapidly diluted in the air and ventilated through the hood (S=2). An audible alarm goes off if vent hood fails, alerting the operator to extinguish combustion. The risk of a leak is low (O=3) because the test section will be tightened with torque wrench and will be pressure tested after every reassembly (D=5). The total RPN for this failure mode is 30, which is acceptable.

Hydrogen Leak in Flow Loop: The entire flow loop is located within a vent hood. Any leaks would be rapidly diluted in the air and be ventilated through the hood (S=2). An audible alarm goes off if vent hood fails, alerting the operator to extinguish combustion. The risk of a leak is low (O=3) because the flow loop has been pressure tested to 50psi and will be retested after fitting adjustments (D=5). The total RPN for this failure mode is 20, which is acceptable.

Power Failure: When electrical power fails in the facility, the vent hood is shut off along with the LabVIEW program, active sensors, and flow controllers. In this situation, the flow of hydrogen is automatically turned off by the normally-closed solenoid valve while the air line is kept open in order to cool the apparatus (S=2). This is expected to be of very low occurrence (O=1) and it is impossible to detect in advance (D=10). The total RPN for this failure mode is 20, which is acceptable.

Unreacted Hydrogen in Exhaust: The entire flow loop is located within a vent hood. Any unreacted hydrogen will be diluted to less than 2% by volume in air (S=1), which is

less than its lower flammability limit (4%). This is expected to happen regularly (O=10) as this will occur during start up and if combustion goes out during an experiment. It will also be readily detectable based on the readings of the thermocouples (D=5). The total RPN for this failure mode is 20, which is acceptable.

5 Experimental Results and Discussion

5.1 Experimental Matrix

In the testing done by Haley [1] and Ghazvini [2], the temperature at which combustion occurs and the residence time of the fuel/air mixture over the catalyst bed had the greatest effect on the hydrogen conversion rates. To determine the fluid mechanics governing the changes, a parametric study will be performed using the conditions described in the experimental matrix below.

Table 4 - Experimental Matrix

	Body Temperature (°C)	Flow Rates (sccm)		
Square Channel	50	200	400	600
	100			
	150			
Large Pins	50	200	400	600
	100			
	150			
Small Pins	50	200	400	600
	100			
	150			

5.2 EDAX Results

While EDAX analysis was performed on three different pins to determine spatial platinum loading trends, (two large 1 mm pins and one small 0.5 mm pin) only one of the large pins was examined in great detail. After fully characterizing the first pin using a relatively fine grid spacing, less resolved data was obtained for the others as the coarse

distributions were found to be sufficient. Eight EDAX data points were taken at 45 degree intervals around the pin of interest, each at 750 µm away from the pin center. The data was collected for each point using a 500X magnification setting on the SEM, which resulted in a square target area with an edge length of about 250 µm. SEM pictures of each location where data was collected are shown in Figure 17, along with a 100X magnification image of the pin of interest.

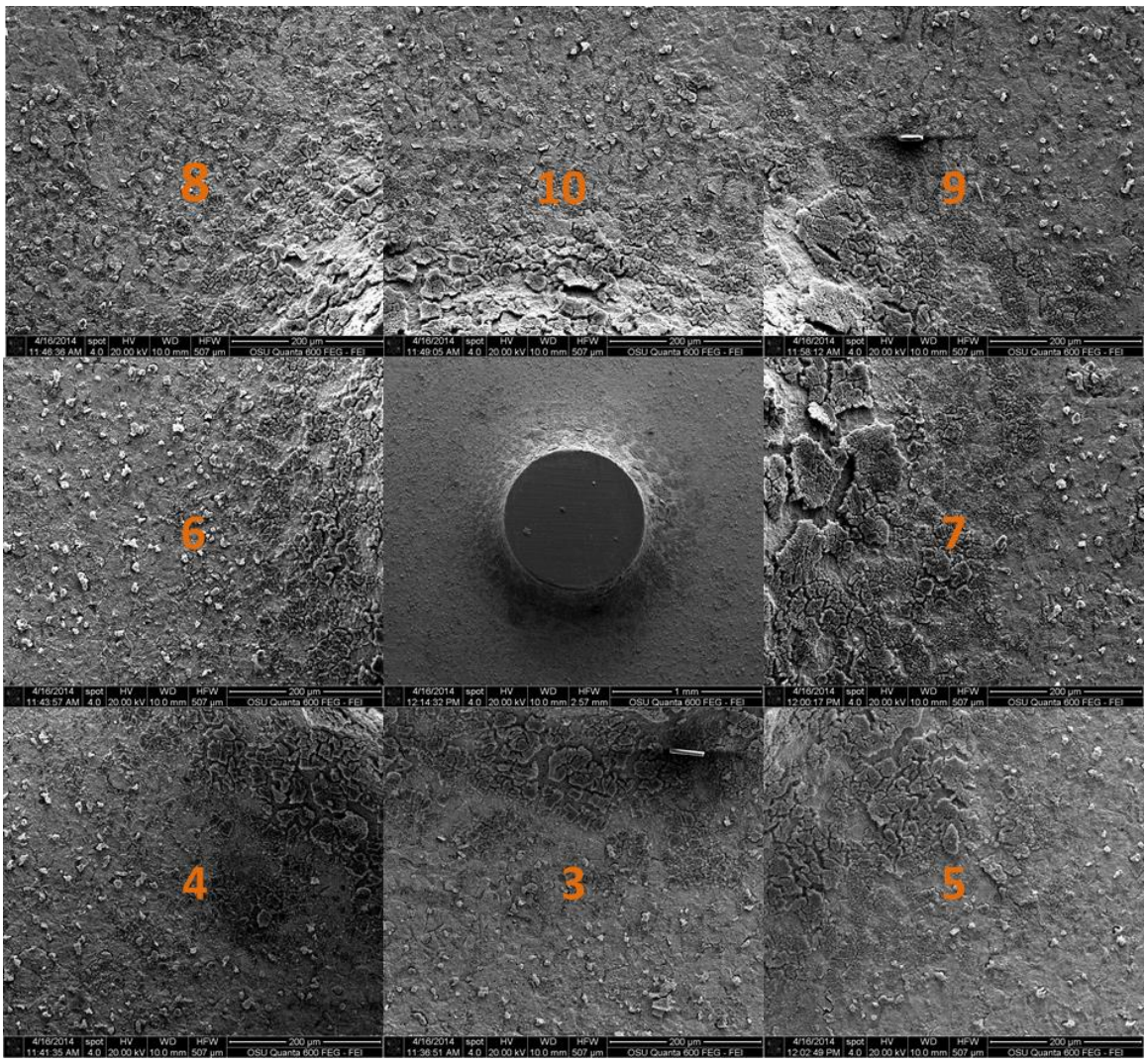

Figure 17 - SEM Pictures of a Large Pin (100X Magnification) and Surrounding Catalyst Regions (500X Magnification) Numbered in Accordance with Figure 16 in Section 4.4.8

EDAX data was also collected at four additional points, two upstream and two downstream of the pin at 1 mm and 1.5 mm away from the pin center. These areas are of interest since the flow will tend to stagnate in as it reaches the front of the pin, causing higher local residence times and thus additional hydrogen conversion. On the downstream side of the pin, the flow tends to form a turbulent wake region, where mixing occurs that produces increased hydrogen conversion rates. Locations where EDAX data was taken are detailed in Figure 16 in Section 4.4.8.

The EDAX device counts the number of x-rays that it detects emitting from the sample and plots them on a histogram according to their energy level. Since the energy levels of the x-rays are characteristic of the emitting element, the relative abundances of each element known to exist in the sample can be measured. An example of the EDAX output (taken from Point 4) is shown in Figure 18. Platinum, oxygen, and known constituents of stainless steel are called out in the plot. Some metallic elements have more than one x-ray energy level associated with them due to the multiple shells of electrons available at higher atomic weights.

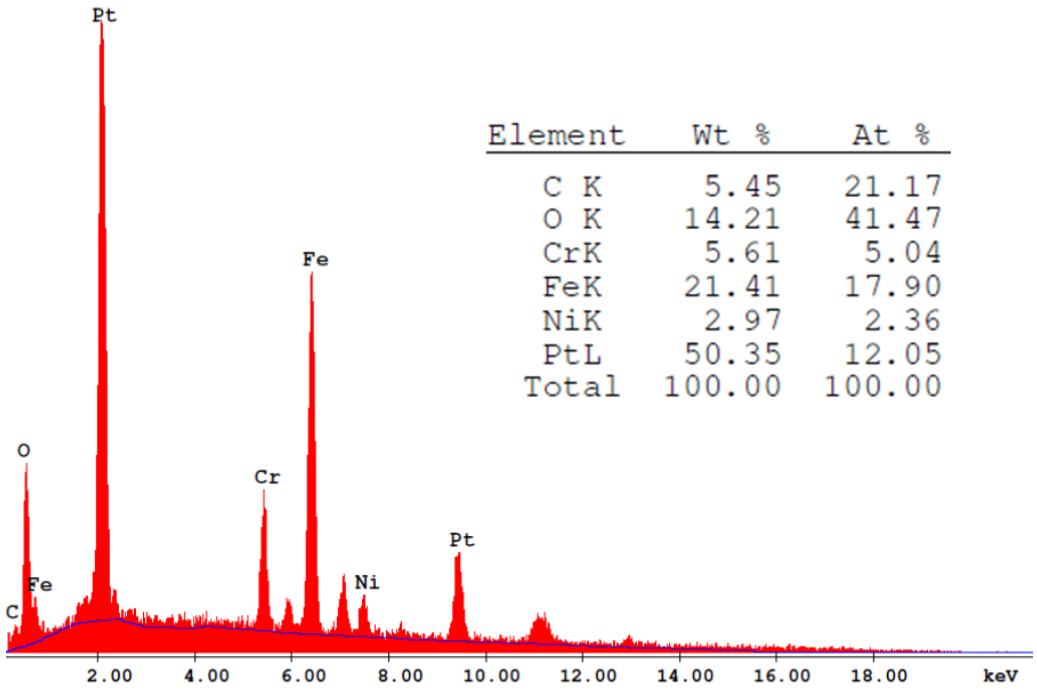

Element	Wt %	At %
C K	5.45	21.17
O K	14.21	41.47
CrK	5.61	5.04
FeK	21.41	17.90
NiK	2.97	2.36
PtL	50.35	12.05
Total	100.00	100.00

Figure 18 - EDAX Histogram and Composition Output (Point 4 on Figure 16)

The weight percentage of platinum and oxygen measured at each of the 12 locations detailed in Figure 16 were plotted as a function of the distance from the center of the pin in the flow direction to visualize the distribution of platinum and oxygen around the pin in Figures 20 and 21. The distribution of oxygen is of interest because platinum oxide does not participate in the catalytic reaction. A high concentration of oxygen in a region where there is a high concentration of platinum can indicate that the region is not particularly active due to the presence of the inactive platinum oxide. This information will be used to evaluate the temperature distributions measured by the IR camera and determine if temperature differences are a result of fluid mechanics or uneven catalyst distribution.

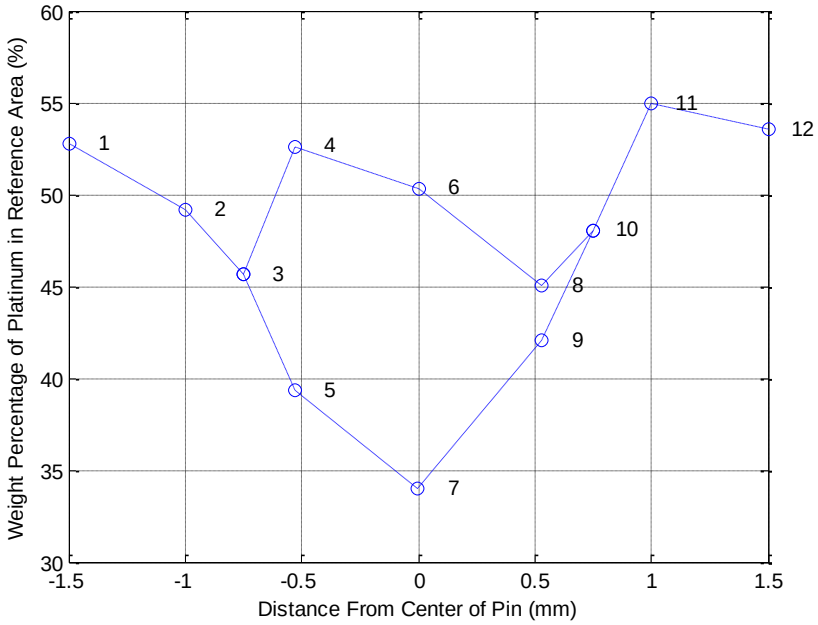

Figure 19 - Distribution of Platinum Around 1mm Pin by Weight Percent According to the Locations Defined in Figure 16 with Flow in the Positive X direction

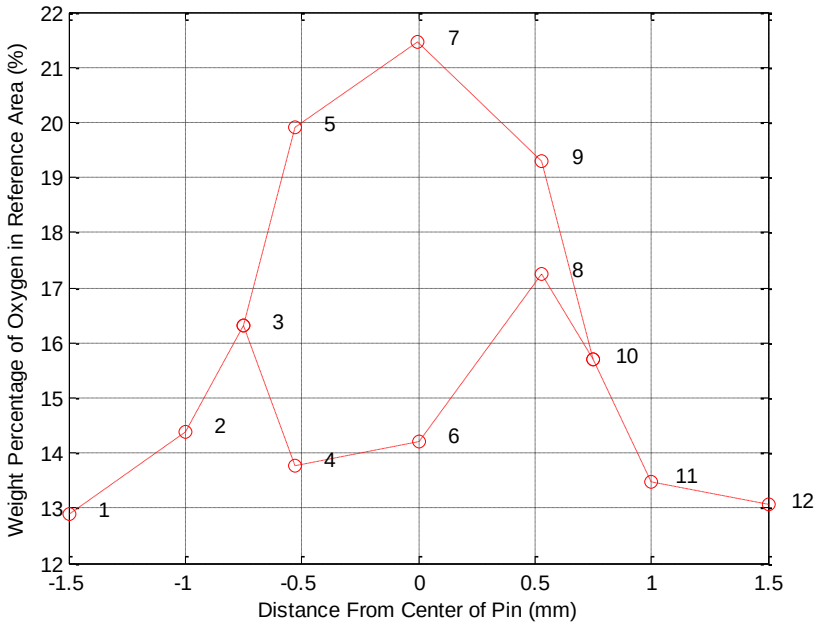

Figure 20 - Distribution of Oxygen Around 1mm Pin by Weight Percent According to the Locations Defined in Figure 16 with Flow in the Positive X direction

The platinum distribution around the pin of interest varies by approximately 38% of its maximum value, with one side containing significantly more platinum than the other. The opposite trend was observed in the distribution of oxygen, with the platinum rich side of the pin containing less oxygen than the platinum poor side.

5.3 Infrared Camera Photographs

The images presented in the following subsections are organized in three groups of eighteen images, each representing a different channel geometry. Nine images in each group of eighteen depict the absolute temperature distribution in the channel. The other nine represent the same data, but are non-dimensionalized by the body thermocouple temperature according to Equation 8.

$$T_{ND} = \frac{T_{Measured}}{T_{Body}} \tag{8}$$

Non-dimensionalization accounts for biasing of the temperature distribution due to slight differences in the test section body temperature at the time the picture was taken. Each collection of nine pictures is organized into a 3 x 3 grid, with each row representing a single body temperature and each column representing a single flow rate. The number in the bottom right hand corner of each image represents the average catalyst temperature in degrees Celsius. Temperatures measured inside the pins are neglected in this measurement. Comparisons between images in the same row are always valid since they share the same color scale. Comparisons between images in the same column are only valid using the non-dimensionalized data, as all rows share the same color scale.

5.3.1 Square channel

5.3.1.1 Infrared Temperature Profiles

The absolute temperature data in Figure 21 appears to indicate that the catalyst bed is cooler at higher flow rates, particularly at 50°C and 100°C. Some uneven catalyst distribution is visible as cool spots, particularly in the 100°C and 150°C ranges. A hot spot appears in the upper right corner of the target area that becomes increasingly prominent at higher flow rates and higher body temperatures.

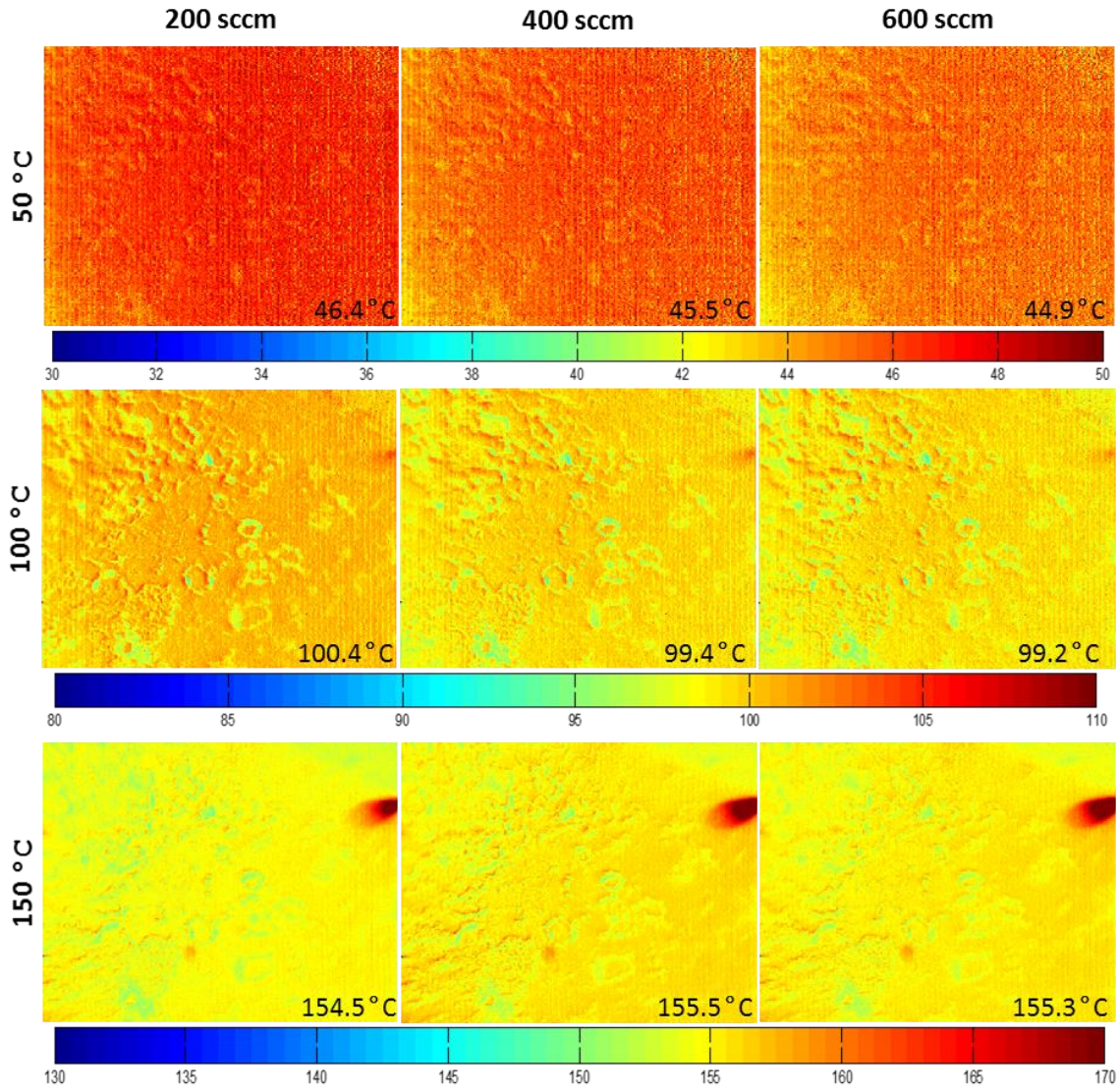

Figure 21 - Absolute Temperature Profiles for Plain Square Channel (Flow Direction Right to Left)

The non-dimensionalized images in Figure 22 indicate that the decreasing temperatures with increasing flow rate trend seen in the absolute temperatures may have been due to slight temperature differences as measured by the body thermocouple. Virtually no flow rate trend is discernable from the non-dimensionalized pictures. Uneven catalyst distribution is still visible, as is the hot spot in the upper right corner.

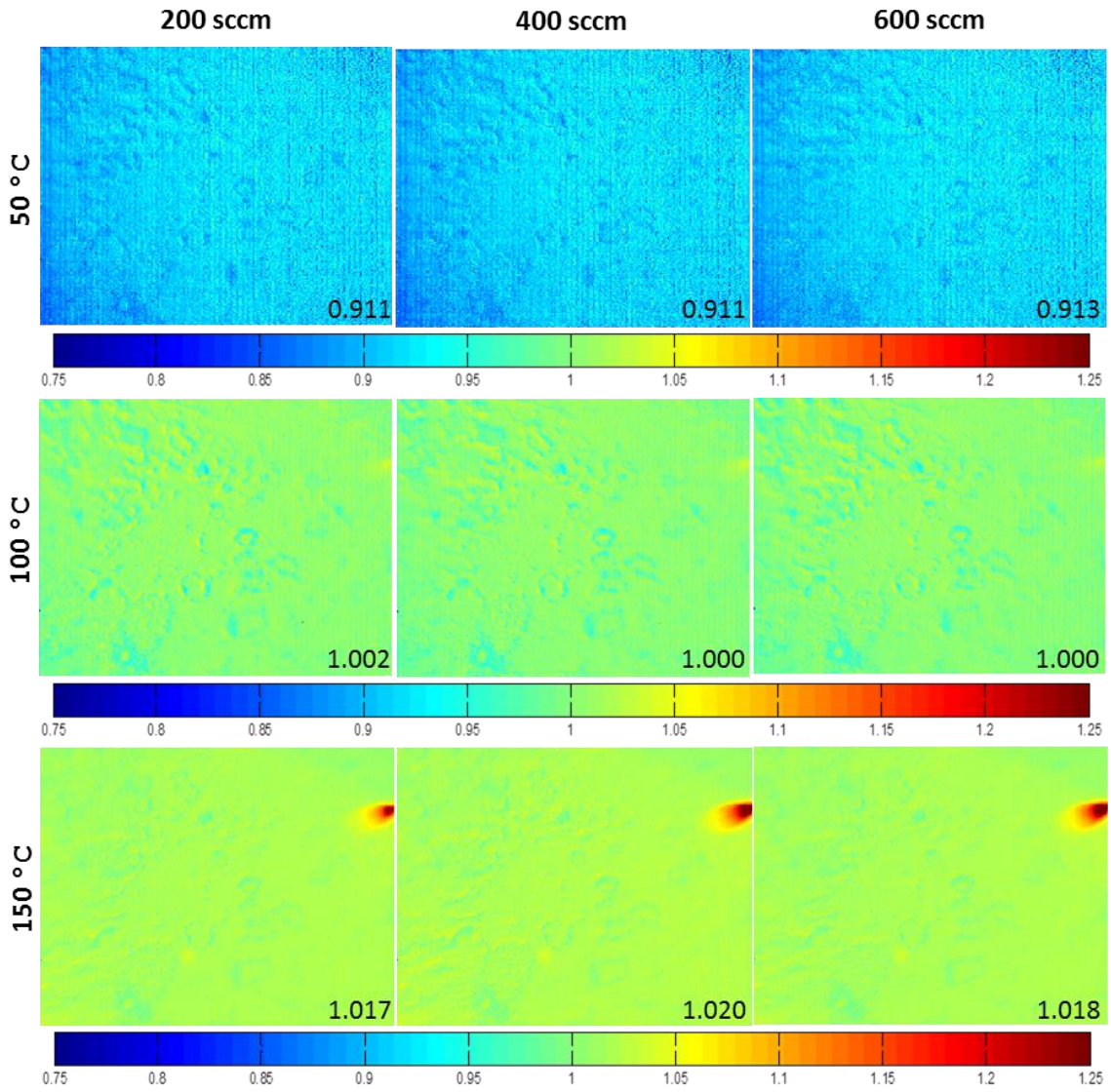

Figure 22 - Non-Dimensionalized Temperature Profiles for Plain Square Channel (Flow Direction Right to Left)

5.3.1.2 Hydrogen Conversion

The hydrogen conversion rates depicted in Figure 23 generally increase with body temperature and decrease with flow rate. The 150 °C data point for a 200 sccm flow rate drops off below the conversion rates of the higher flow rates, which does not match the

other trends. The conversion rates have very similar slopes, indicating that the effect of flow rate offsets the conversion rates by a certain value. Conversion rates range from approximately 35% at 50°C up to 75% at 150°C. The error is relatively high for two of the 600 sccm data points, while it is nearly insignificant in all others.

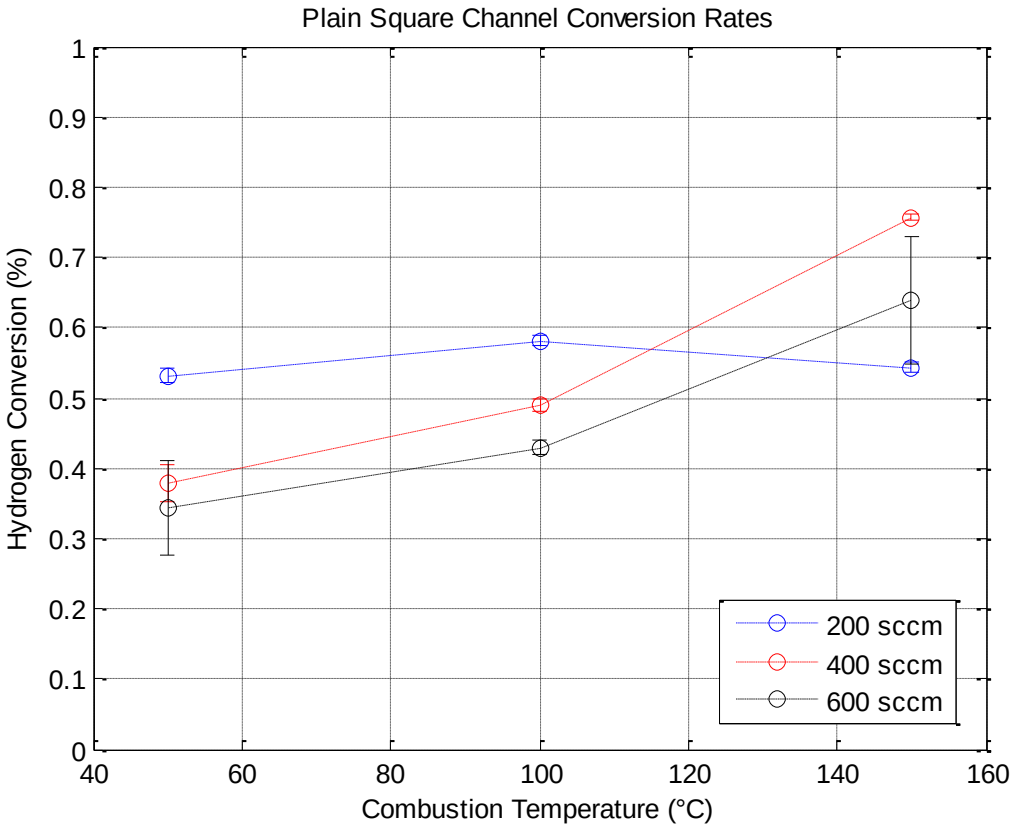

Figure 23 - Hydrogen Conversion Rates as a Function of Temperature and Flow Rate for Plain Square Channel

5.3.2 Large pin fin channel

5.3.2.1 Infrared Temperature Profiles

The pin is clearly visible in the absolute temperature images shown in Figure 24, but the temperature values within the pin boundaries no not represent real temperatures as the surface of the pin is outside of the focal plane of the IR camera lens. The 50°C row is very grainy and exhibits no trend with flow rate. The 100°C and 150°C rows appear to exhibit opposite trends, with the 100°C row temperature decreasing with flow rate while the opposite is true for the 150°C row. The non-uniformity of catalyst distribution is more apparent at higher temperatures. No flow enhancement due to the pin is visible as a higher temperature region.

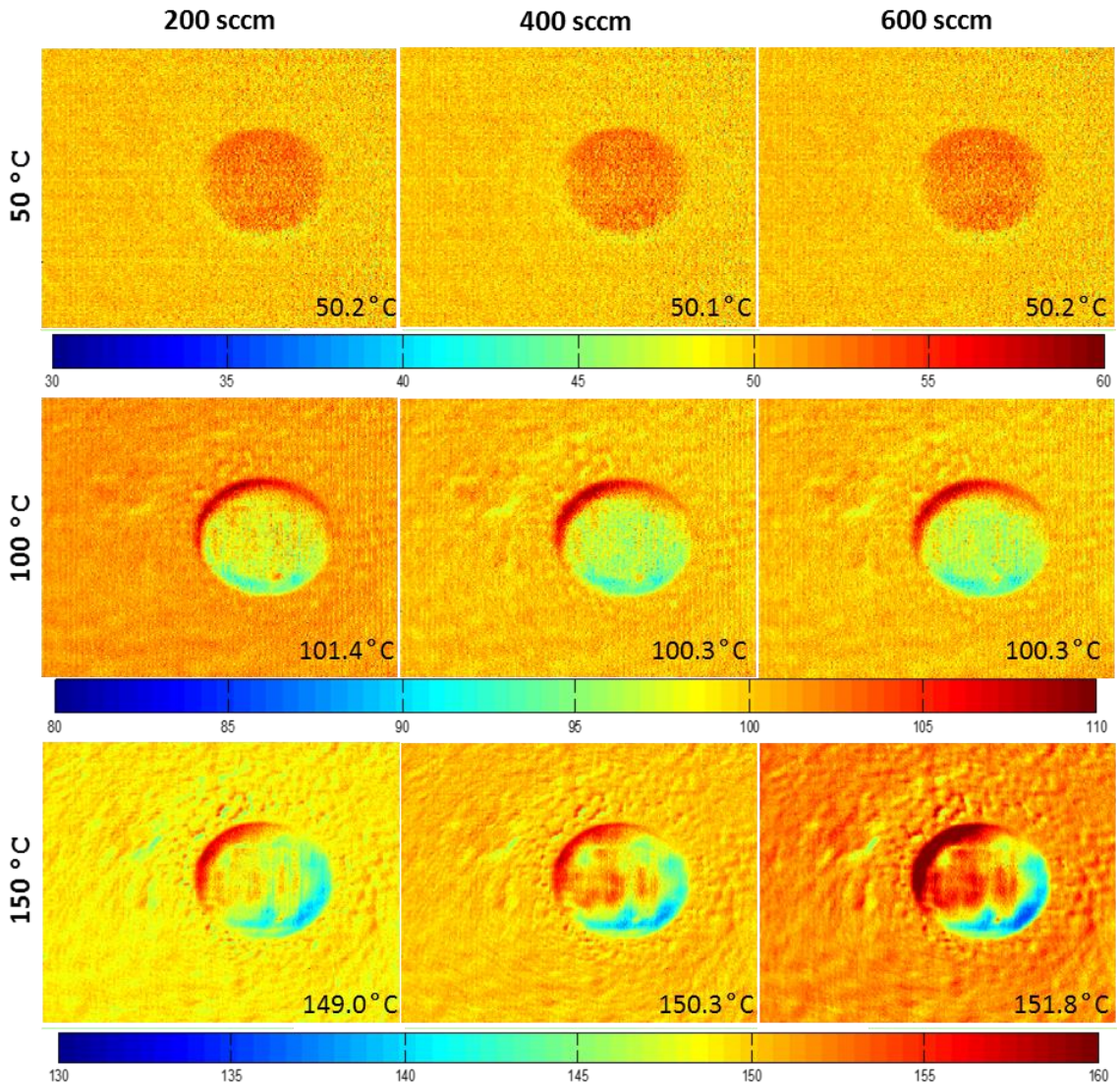

Figure 24 - Absolute Temperature Profiles for 1 mm MPFA Channel (Flow Direction Right to Left)

The non-dimensionalized images in Figure 25 appear to make the 50°C row even grainier than the absolute temperature data. Again, the temperatures within the pin boundaries are meaningless as the pin surface was not in focus. The only visible trend is decreasing non-dimensional temperatures as body temperature is increased. This may be due to the graininess of the images at lower body temperatures.

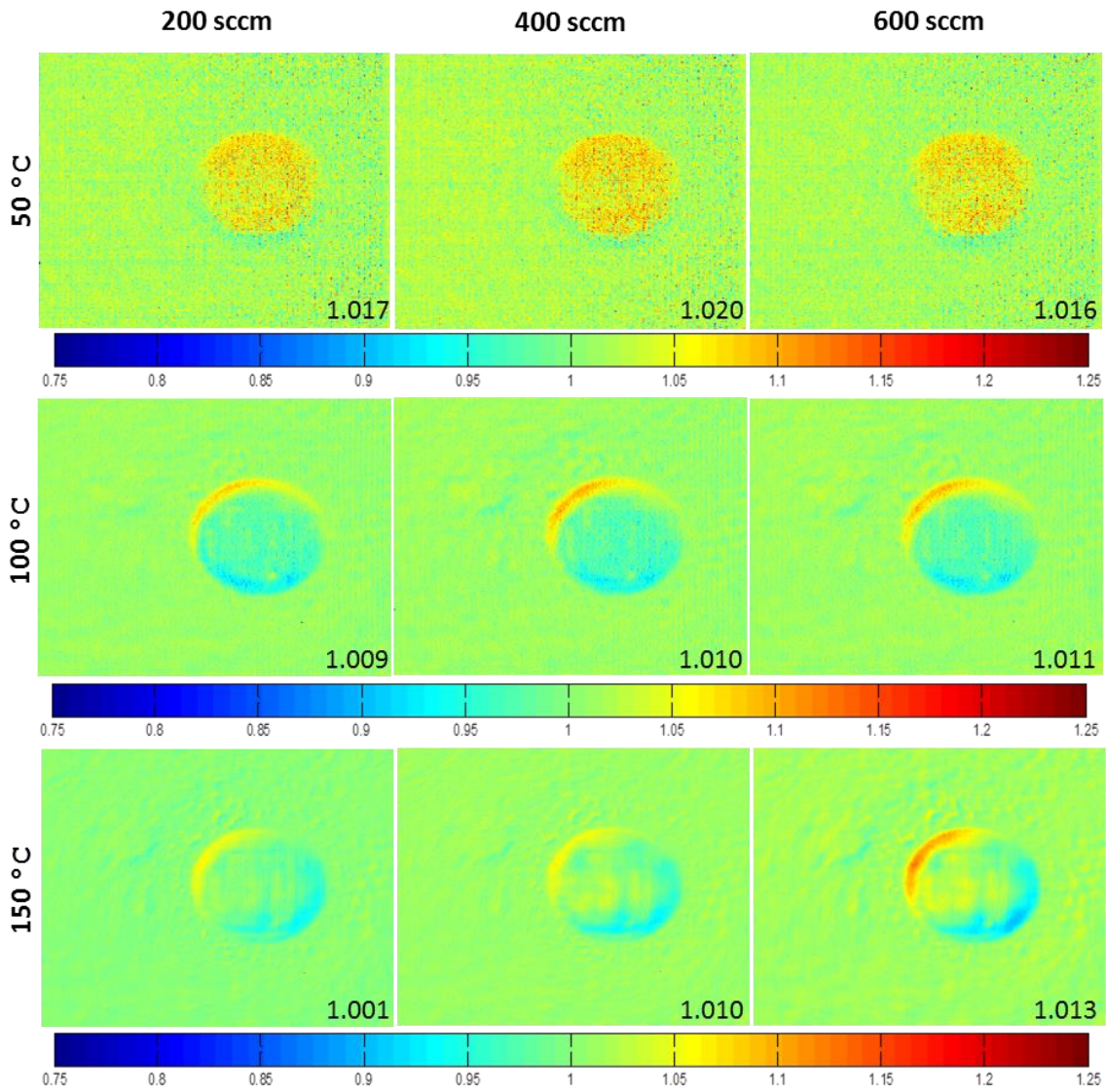

Figure 25 - Non-Dimensionalized Temperature Profiles for 1 mm MPFA Channel (Flow Direction Right to Left)

5.3.2.2 Hydrogen Conversion

Hydrogen conversion rates plotted in Figure 26 appear to be highest at low flow rates (200 sccm) and high temperatures (150°C). The conversion rate increases as temperature increases and to a lesser extent increases as flow rate decreases. The error of the

conversion measurements is highest in the 600 sccm flow rate region, and the 100°C 400 sccm data point has unusually high error. The entirety of the error arises due to the variation in repeatability of the gas chromatograph. Large uncertainties suggest that the sample bag may have been contaminated with leftover gasses from other samples.

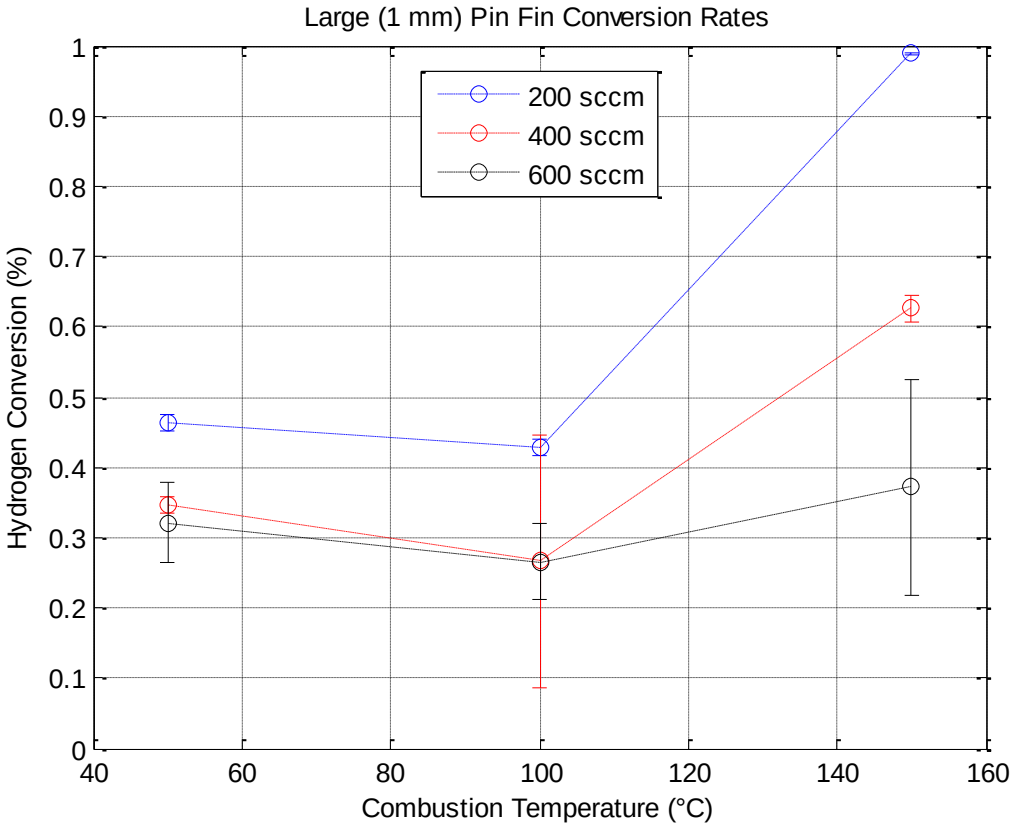

Figure 26 - Hydrogen Conversion Rates as a Function of Temperature and Flow Rate for 1 mm MPFA Channel

5.3.3 Small pin fin channel

5.3.3.1 Infrared Temperature Profiles

The pin of interest is clearly visible as the rightmost pin in the center of the images shown in Figure 27. The temperature appears to decrease as the flow rate is increased in the 50°C and 100°C regions, while it appears to increase slightly with flow rate in the 150°C row. The trend is particularly dramatic in the 100°C row. No flow enhancement phenomena caused by the pins is visible in the temperature data. Some uneven catalyst distribution is visible in the top right of the images. As with the large pin data, the temperatures within the pin boundaries are meaningless because the pin surfaces are outside of the focal plane of the camera.

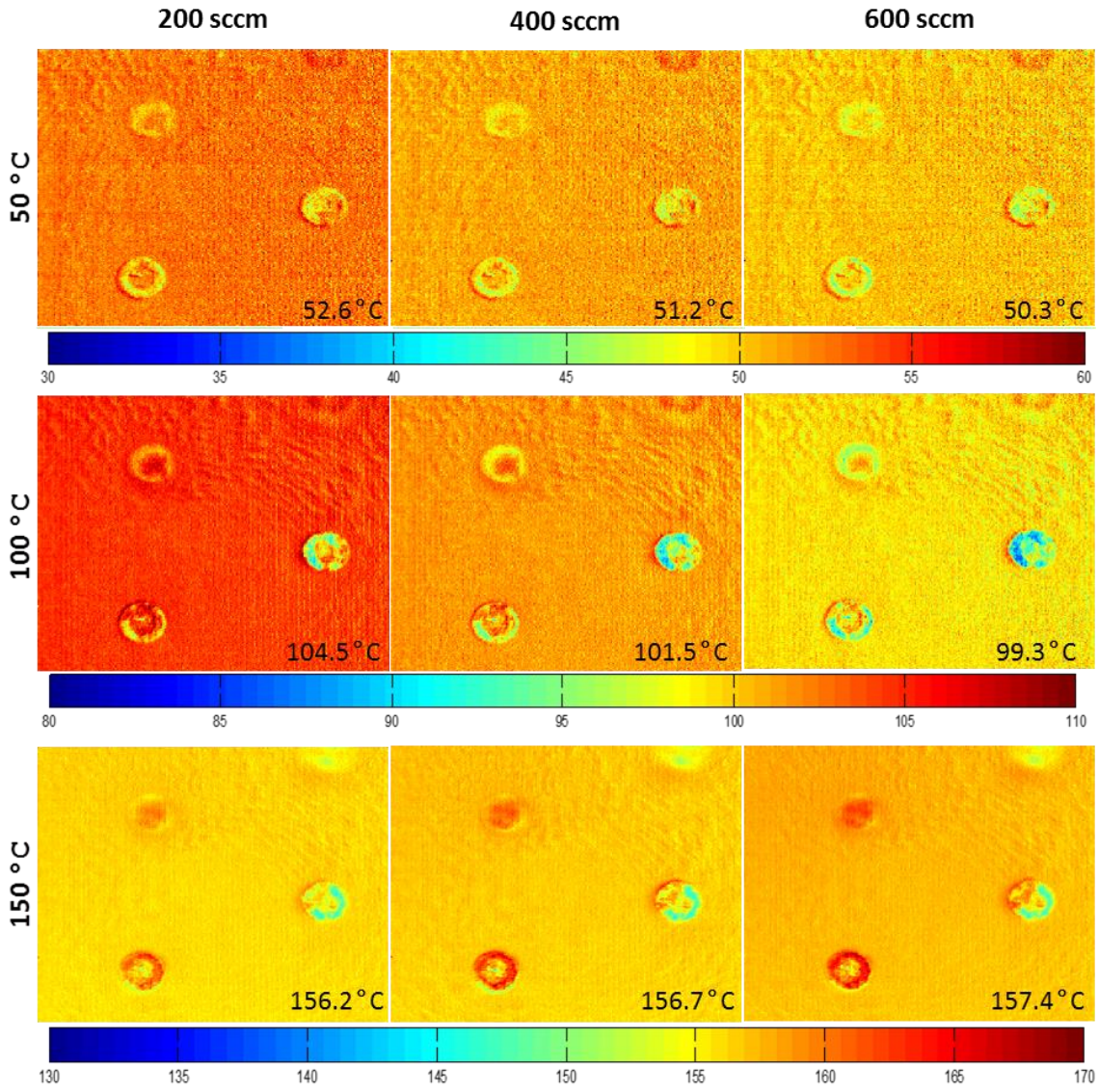

Figure 27 - Absolute Temperature Profiles for 0.5 mm MPFA Channel (Flow Direction Right to Left)

The non-dimensionalized images exhibit much less difference between rows than the absolute temperature data in Figure 28. There appears to be a slight trend of increasing channel surface temperature as the body temperature is increased. In the 150°C row the temperature appears to increase slightly as flow rate is increased.

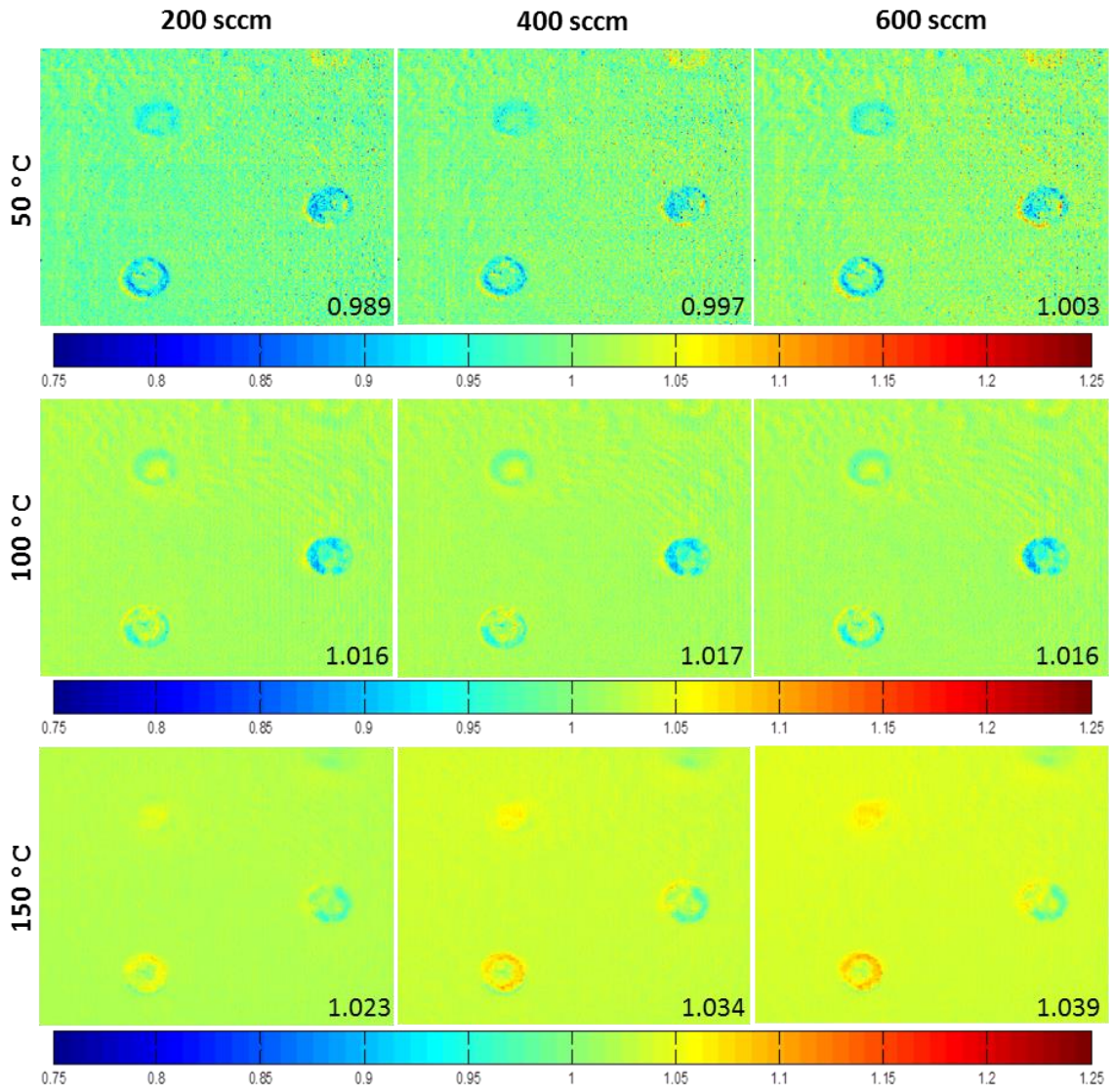

Figure 28 - Non-Dimensionalized Temperature Profiles for 0.5 mm MPFA Channel (Flow Direction Right to Left)

5.3.3.2 Hydrogen Conversion

The hydrogen conversion rates of the 0.5 mm MPFA channel appear to not change very much with respect to temperature, as for all flow rates the difference remains within 10% of the 50°C conversion rate as seen in Figure 29. The 200 sccm conversion rate is slightly

higher than the larger flow rates, which overlap in the 100°C range. The error is again high for the 600 sccm flow rate, particularly in the 100°C data point where the error is nearly as large as the actual value of the measurement. Again, all uncertainty associated with the GC measurements arises due to variations in the repeatability of the instrument when measuring the exact same sample of gas. It is likely the sample taken at 100°C and 600 sccm was contaminated with exhaust gasses from another sample.

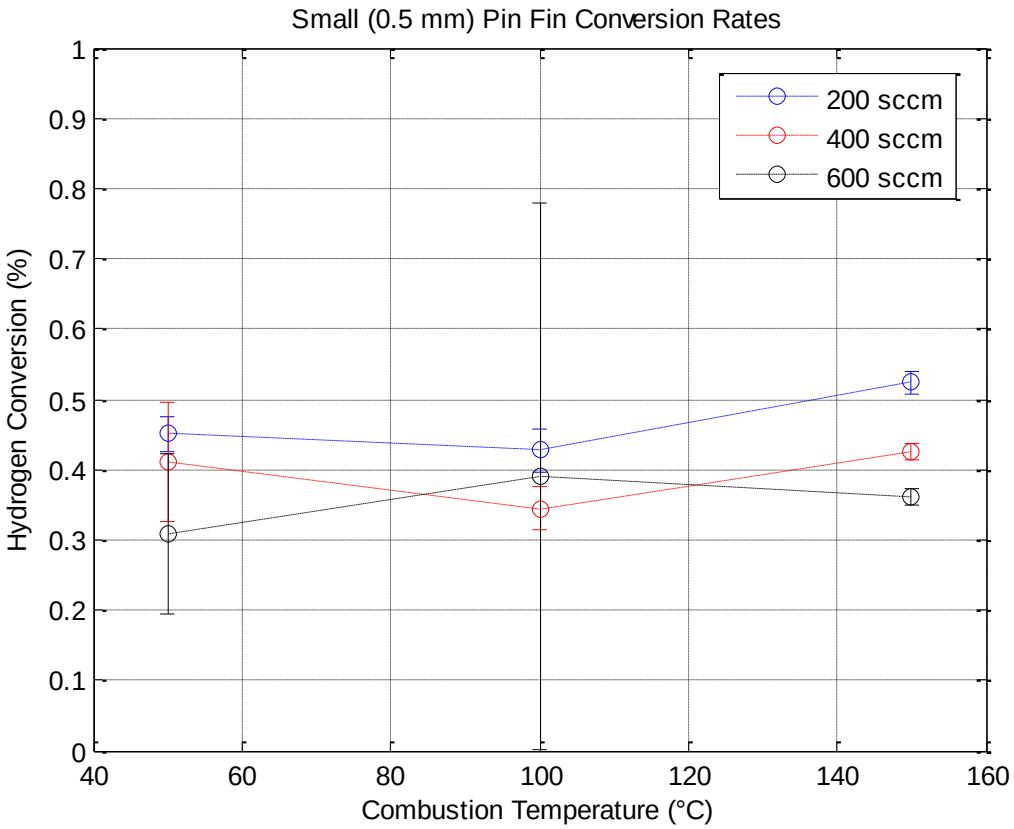

Figure 29 - Hydrogen Conversion Rates as a Function of Temperature and Flow Rate for 0.5 mm MPFA Channel

5.3.4 Comparison

Comparison of the infrared images obtained using the three different channel configurations can be done using the non-dimensionalized images since all of them are scaled equally. The hydrogen conversion rates can also be compared numerically. In each case, the catalyst activity may be different for each shim and must be considered when comparing the temperatures and hydrogen conversion rates of each shim.

The hydrogen conversion rates plotted in Figure 30 appear to be best for the square channel for the lower temperatures while the 1 mm MPFA generates a very high conversion rate at 150°C. The severe increase in conversion rate at this single data point indicates that the measurement may have been in error since it is much larger than other conversion rates observed during experimentation at any flow rate.

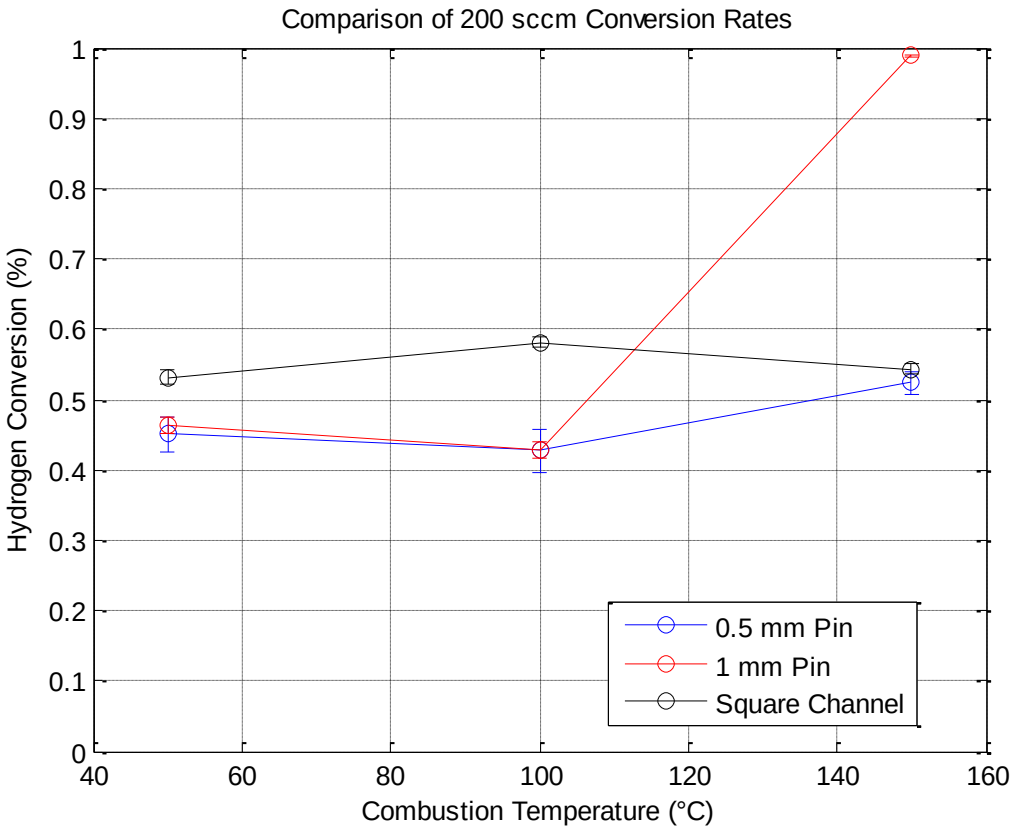

Figure 30 - Comparison of Channel Geometries at a Flow Rate of 200 sccm

The plain square channel appears to dominate the hydrogen conversion rates among the three channel geometries at temperatures above 50°C, while the large 1 mm pin also begins to increase dramatically above 100°C according to the data plotted in Figure 31. The conversion rates of the 0.5 mm MPFA remain relatively constant over all temperatures.

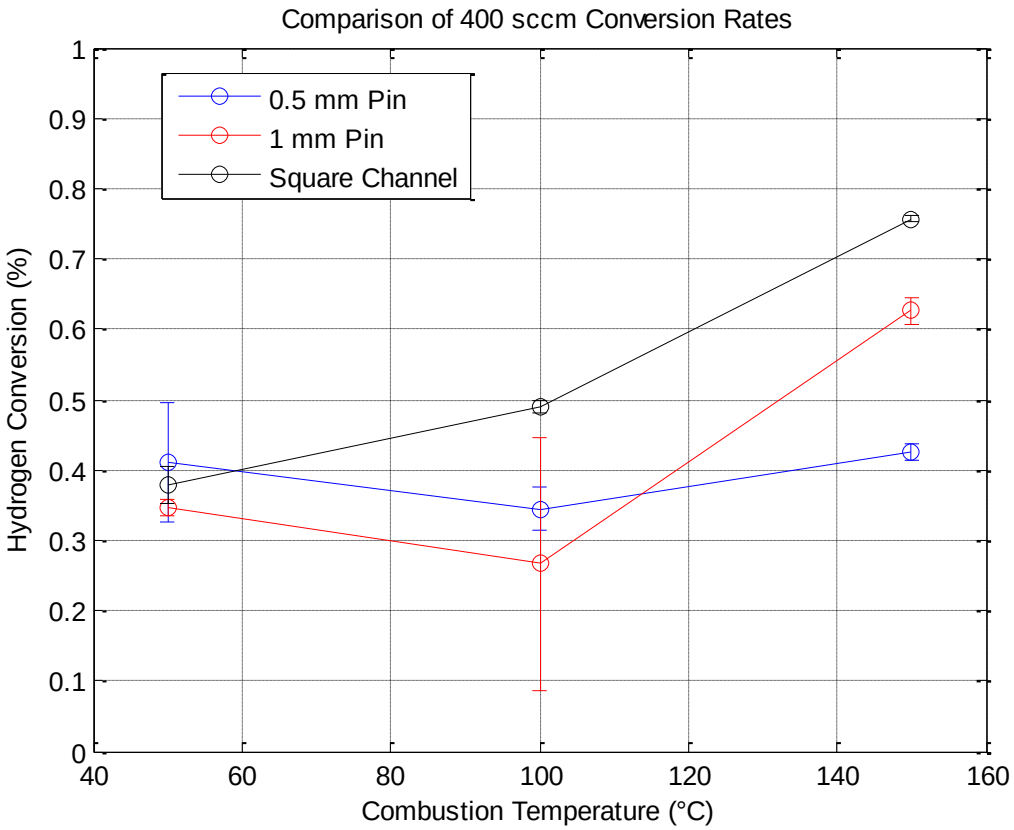

Figure 31 - Comparison of Channel Geometries at a Flow Rate of 400 sccm

Again, the plain square channel produces the highest hydrogen conversion rates, this time at all body temperatures. However, the large error in the 100°C data point for the 0.5 MPFA shim may place its conversion rate above that of the plain square channel as evidenced in Figure 32. The error for all three shims at the 600 sccm flow rate is relatively large compared to the lower flow rates, as is the magnitude of the conversion.

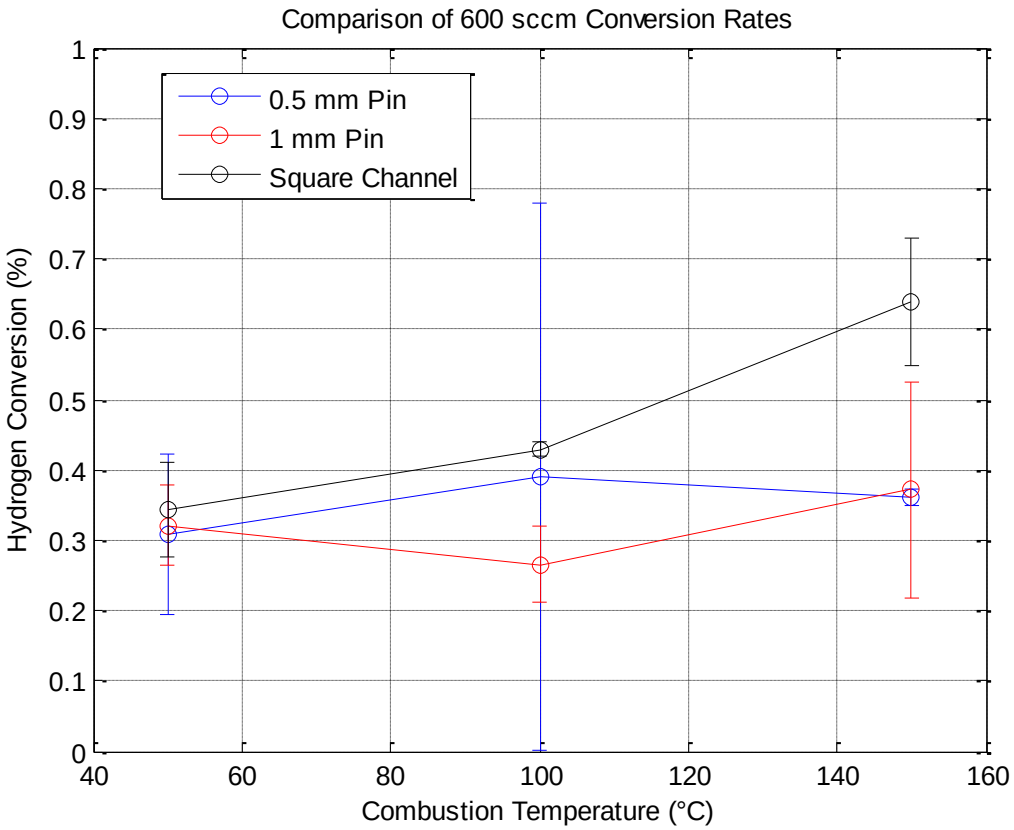

Figure 32 - Comparison of Channel Geometries at a Flow Rate of 600 sccm

In the following figures, the three channel geometries will be compared at each body temperature. Direct comparisons are possible since the non-dimensionalized images are all at the same scale (0.75-1.25).

The plain channel appears to be much cooler than the channels with pin fins in the images shown in Figure 33. The 1 mm MPFA appears to be slightly warmer than the 0.5 mm array, indicating that it may have higher conversion rates. According to the GC measurements this is true in the 200 and 600 sccm conditions but not in the 400 sccm condition.

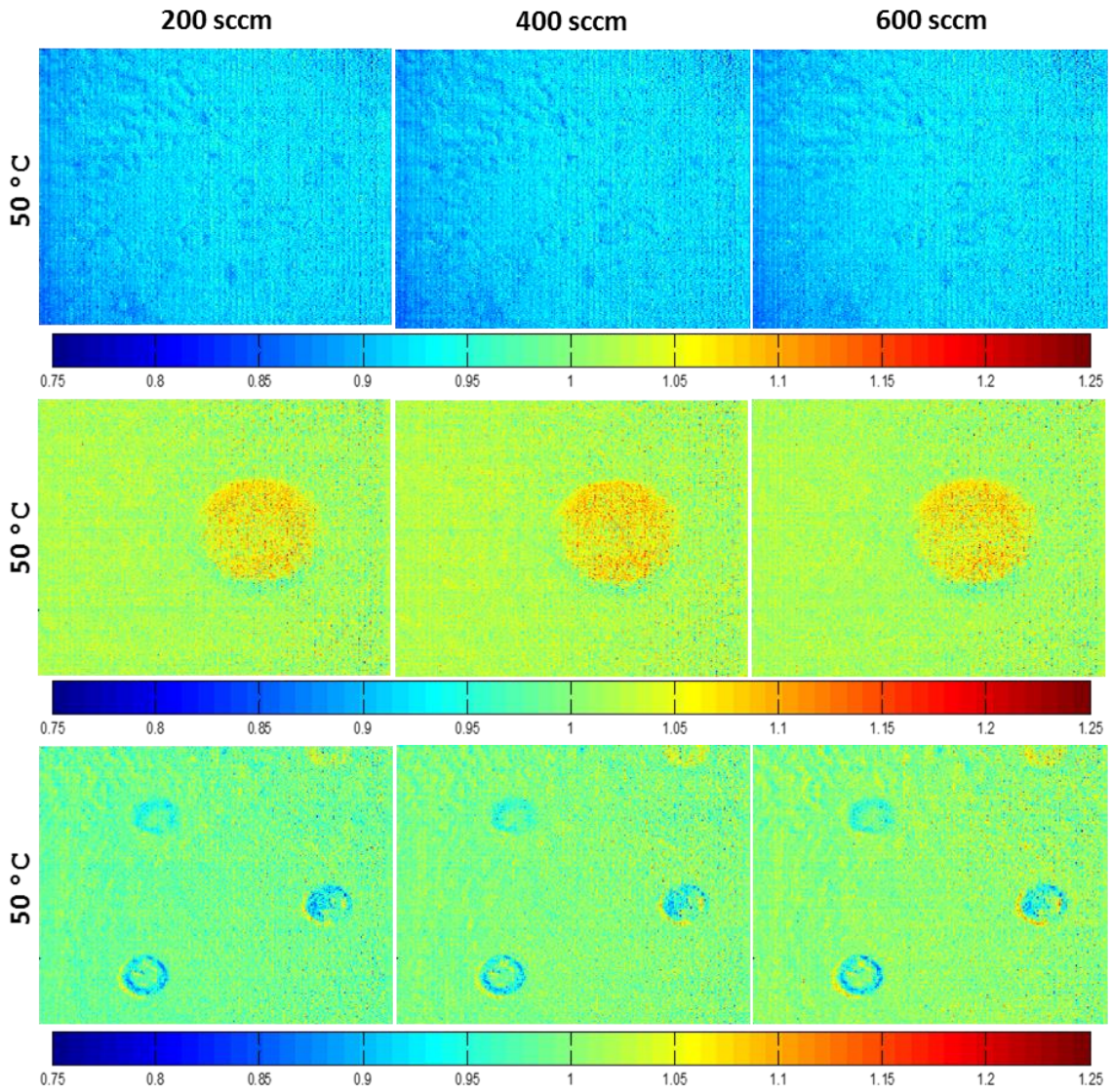

Figure 33 – Non-Dimensional Comparison of Channel Geometries at 50 °C

The non-dimensional temperature profiles in Figure 34 appear to be roughly equivalent at a body temperature of 100°C, indicating that they all have roughly the same hydrogen conversion rates. However, the disparity between the measured conversion rates is much higher than any flow rate at 50°C, meaning that the temperature distribution may not be a good indicator of hydrogen conversion rates.

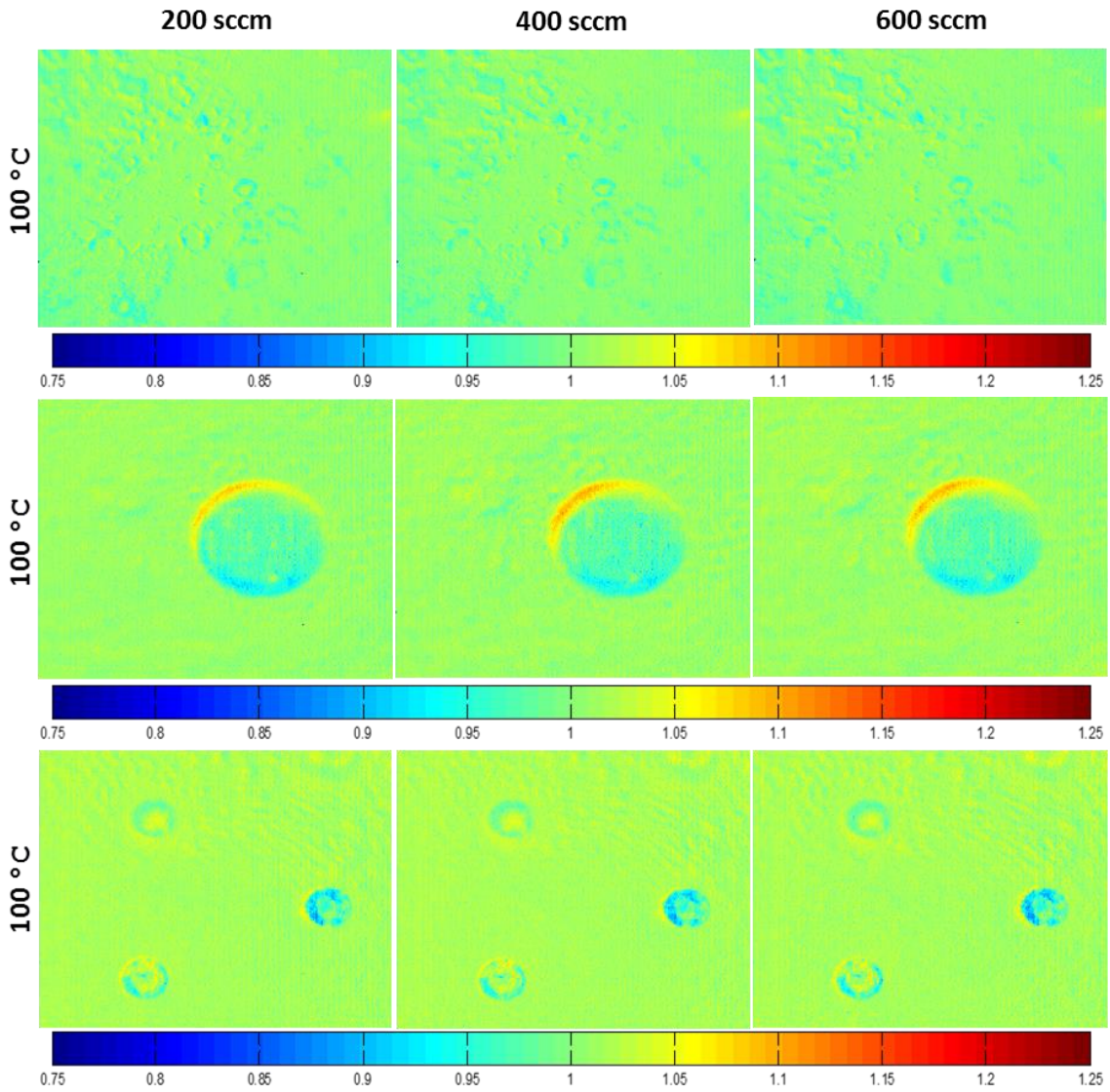

Figure 34 - Non-Dimensional Comparison of Channel Geometries at 100°C

The plain square channel and 0.5 mm MPFA geometries appear to generate slightly hotter channel surfaces at 150°C than the 1 mm MPFA as seen in Figure 35. However, the hydrogen conversion data indicates that this is only true in the case of the plain square channel. The 1 mm MPFA always has better hydrogen conversion performance than the 0.5 mm array at 150°C, again indicating that the temperature distribution is not necessarily a good indicator of hydrogen conversion performance.

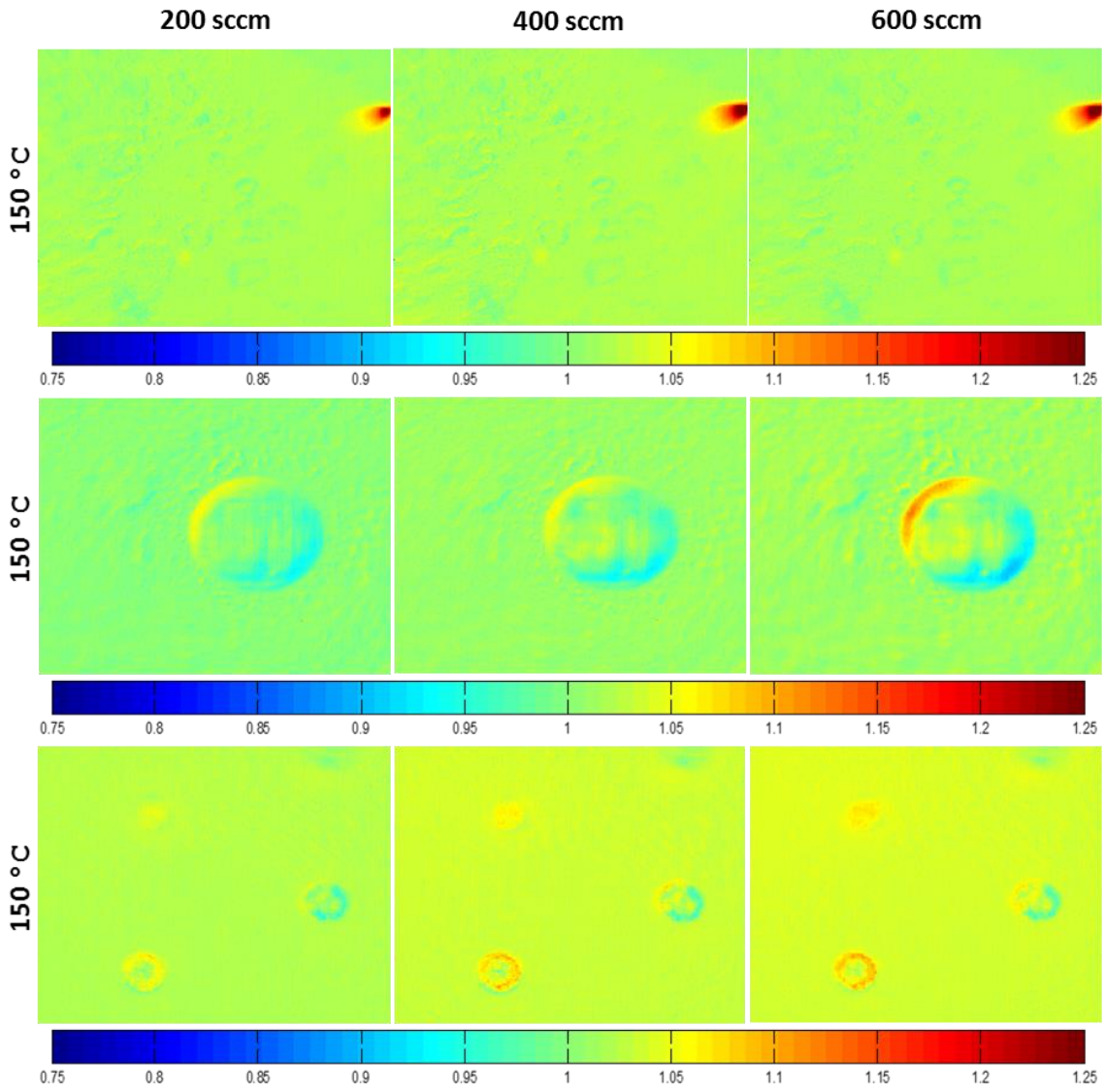

Figure 35 - Non-Dimensional Comparison of Channel Geometries at 150°C

6 Conclusion and Final Remarks

6.1 Conclusion

The infrared images gathered during testing indicate that the methodology used to capture the pictures does not produce images that can provide any insight into the efficacy of the MPFA. The lack of useful infrared data most likely arose from the use of the test section heater during data collection. The output from the heater is much larger than the heat generated by combustion, eliminating any spatial temperature gradients caused by the pin fins. In order to visualize the desired flow effects, the heater must be turned off and the temperature profile generated by the combustion allowed to reach steady state. Unfortunately, the reaction does not produce enough heat to be self-sustaining at a constant temperature, so any pictures taken using this method will not be at steady state conditions.

The lack of spatially varying temperature in the infrared images makes interpreting the EDAX and SEM measurements difficult. Any effect the distribution of catalyst had on the temperature profile was likely obscured by the overpowering effect of the heater. While turning off the heater may provide more insight into how the catalyst distribution affects conversion performance, a more direct measurement of catalyst activity is needed. A chemisorption technique can directly measure the activity of a catalyst by reacting a gas of known composition and very accurately measuring how much remains unreacted after a certain time interval.

The results of gas chromatography are not directly comparable to the IR, EDAX, and SEM results as the exhaust gas composition is measurement of the overall performance of the catalyst, while the other measurement techniques focus on a small region of the catalyst. The gas chromatography results were fairly inconsistent, particularly in terms of the large variability in the error caused by the GC itself. The error likely arises due to contaminated or leaky sample bags, as the data points with unacceptable error were taken in between others with excellent error values, indicating a problem somewhere between the sample collection and the GC. The inability to get repeatable data on different days is very concerning. The catalyst appears to degrade rapidly if left in the open air. The mechanism of degradation is likely absorption of water vapor from the air by the very dry catalyst surface, effectively reversing the effect of calcining. Potential solutions to the catalyst deactivation problem include developing a new deposition technique or simply storing the activated catalyst in an inert environment. A new deposition technique is suggested, as it may also increase the activity and lifespan of the catalyst.

In light of the inconsistency of results due to inadequate time available to conduct experiments, the analysis framework must be modified in accordance with the suggestions described above to produce meaningful results. The measurement and calibration techniques developed during experimentation and the exposed inadequacies of these procedures provide an excellent starting point for future work in meaningful characterization of micro pin fin arrays in chemical reactors.

6.2 Recommendations for Future Study

With the desire to increase catalytic combustion efficiency in mind, much more work must be done to characterize the full potential of micro pin fin arrays. First, more experimentation should be performed using the geometry described in this work, as constrained time and resources did not allow for thorough characterization of fresh catalyst. The catalyst should be kept out of open air to prevent degradation and the sample bags should be used more carefully to prevent contamination. In addition, a method of directly measuring the activity of the catalyst rather than just its elemental composition should be investigated. The procedure used to capture infrared images should be modified to turn off the heater and allow the heat generated by combustion to develop temperature profiles unhindered by the overpowering heat source.

As the MPFAs geometries used in preliminary testing did not appear to improve the conversion efficiency of hydrogen, different geometries should be investigated. Pins with different diameters, spacing, and stagger configurations should be investigated after consulting literature for near-optimal geometrical parameters. A taller channel would cause a larger percentage of the flow to occur outside of the viscous regions near the walls and may generate a more pronounced effect from the pin fins that could be measured using infrared thermography. Repeatability of hydrogen conversion measurements should be improved by increasing the effective lifetime of the catalyst. Better care should be taken of catalyst after it has been calcined and is outside of the test section to prevent the de-activation seen during repeatability testing.

It may also be of interest to investigate alternative fuels for the combustor, as they may be more influenced by the pin fin flow mechanisms and can allow the catalytic combustion technology to be used in a wider variety of applications.

7 Bibliography

[1] D. B. Haley, "Performance Characterization of an Integrated Microscale Hydrogen Combustor Recuperator and Oil Heat Exchanger," Masters Thesis, Oregon State University, 2011.

[2] M. Ghazvini, "Compact Integrated Microchannel Combustor Recuperator and Heat Exchanger for Hydrogen Storage Applications," PhD Thesis, Oregon State University, 2013.

[3] M. Sato and T. Kobayashi, "A Fundamental Study of the Flow Past a Circular Cylinder using Abaqus/CFD," Mechanical Design & Analysis Corporation, 2012.

[4] F. E. Ames and L. A. Dvorak, "Turbulent Transport in Pin Fin Arrays: Experimental Data and Predictions," vol. 128, 2006.

[5] A. Zukauskas, "Heat Transfer from Tubes in Crossflow," *Advances in Heat Transfer*, vol. 8, pp. 93-160, 1972.

[6] D. E. Metzger, R. A. Berry and J. P. Bronson, "Developing Heat Transfer in Rectangular Ducts with Staggered Arrays of Short Pin Fins," *ASME Journal of Heat Transfer*, vol. 104, pp. 700-706, 1982.

[7] D. Mei, M. Qian, B. Liu, B. Jin, Z. Yao and Z. Chen, "A Micro-Reactor with Micro-Pin-Fin Arrays for Hydrogen Production Via Methanol Steam Reforming," vol. 205, 2012.

[8] N. Zheng, E. G. Seebauer and R. I. Masel, "Effects of Microreactor Geometry on Performace: Differences Between Posted Reactors and Channel Reactors," *Industrial & Engineering Chemistry Research*, vol. 44, pp. 4267-4271, 2005.

[9] M. Planck, The Theory of Heat Radiation, Philadelphia: P. Blakiston's Son & Co., 1914.

[10] C. M. Carlomagno and G. Cardone, "Infrared Thermography for Convective Heat Transfer Measurements," *Experiments in Fluids*, vol. 49, no. 6, pp. 1187-1218, 2010.

[11] S. R. Sargent, C. R. Hedlund and P. M. Ligrani, "An Infrared Thermography Imaging System for Convective Heat Transfer Measurements in Complex Flows," *Measurement Science and Technology*, vol. 9, no. 12, 1998.

[12] M. F. Westby, "Heat Transfer Measurements Using Infra-Red Thermography in Rarefied Flows," Defense Research Agency, Farnborough, 1992.

[13] W. Choi, S. Kwon and H. D. Shin, "Combustion Characteristics of Hydrogen-Air Premixed Gas in a Sub-Millimeter Scale Catalytic Combustor," vol. 33, 2008.

[14] P. K. Das, A. Z. Weber, G. Bender, A. Manak, D. Bittinat, A. M. Herring and M.

Ulsh, "Rapid Detection of Defects in Fuel Cell Electrodes using Infrared Reactive-Flow-Through Technique," *Journal of Power Sources,* 2013.

[15] P. Gelin, L. Urfels, M. Primet and E. Tena, "Complete Oxidation of Methane at Low Temperature Over Pt and Pd Catalysts for the Abatement of Lean-Burn Natural Gas Fueled Vehicles Emissions: Influence of Water and Sulphur Containing Compounds," *Catalysis Today,* pp. 45-57, 2003.

[16] N. M. Kinnunen, M. Suvanto, M. A. Moreno, A. Savimaki, K. Kallinen, T. J. Kinnunen and T. A. Pakkanen, "Methane Oxidation on Alumina Supported Palladium Catalysts: Effect of Pd Precursor and Solvent," *Applied Catalysis,* pp. 78-87, 2009.

[17] A. Tompos, J. L. Margitfalvi, E. Tfirst, L. Vegvari, M. A. Jaloull, H. A. Khalfalla and M. M. Elgarni, "Development of Catalyst Libraries for Total Oxidation of Methane: A Case Study for Combined Application of Holographic Rsearch Strategy and Artifical Neural Networks in Catalyst Library Design," *Applied Catalysis,* vol. 285, no. 1-2, pp. 65-78, 2005.

[18] T. Astarita and G. M. Carlomagno, Infrared Thermography for Thermo-Fluid-Dynamics, New York: Springer Heidelberg, 2013.

[19] P. Stefanov, D. Stoychev, I. Valov, A. Kakanakova-Georgieva and T. Marinova, "Electrochemical Deposition of Thin Zirconia Films on Stainless Steel 316L," vol. 65, no. 2, 2000.

[20] A. E. Schweizer and G. T. Kerr, "Thermal Decomposition of Hexachloroplatinic Acid," vol. 17, no. 8, 1978.

[21] M. T. Janicke, H. Kestenbaum, U. Hagendorf, F. Schuth, F. Maximiliam and K. Schubert, "The Controlled Oxidation of Hydrogen from an Explosive Mixture of Gases Using a Microstructured Reactor/Heat Exchanger and Pt/Al2O3 Catalyst," vol. 191, 2000.

[22] D. G. Norton, E. D. Wetzel and D. G. Vlachos, "Thermal Management in Catalytic Microreactors," vol. 45, no. 1, 2006.

[23] W. R. Schwartz, D. Ciuparu and L. D. Pfefferle, "Combustion of Methane over Palladium-Based Catalysts: Catalytic Deactivation and Role of the Support," *Journal of Physical Chemistry,* pp. 8587-8593, 2012.

[24] N. Mouaddib, C. Feumijantou, E. Garbowski and M. Primet, "Catalytic oxidation of methane over palladium supported on alumina: Influence of the oxygen-to-methane ratio," *Applied Catalysis,* pp. 129-144, 1992.